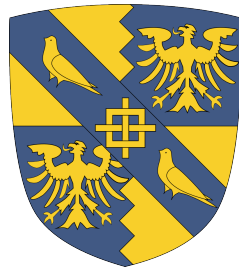


# Kirigami Sheets

## Engineering Objects with Holes



**Spencer R. Wilson**

Department of Engineering  
University of Cambridge  
Supervisor: K.A. Seffen

This dissertation is submitted in partial fulfillment for the degree of  
*Master of Philosophy*

Magdalene College

November 2016



I would like to dedicate this thesis to my awesome parents and friends.  
Thanks for putting up with me.



## **Declaration**

I hereby declare that except where specific reference is made to the work of others, the contents of this dissertation are original and have not been submitted in whole or in part for consideration for any other degree or qualification in this, or any other university. This dissertation is my own work and contains nothing which is the outcome of work done in collaboration with others, except as specified in the text and Acknowledgements. This dissertation contains fewer than 15,000 words excluding appendices, bibliography, footnotes, tables and equations.

Spencer R. Wilson  
November 2016



## Acknowledgements

I would like to thank my supervisor, Dr Keith Seffen for his direction, but also for his open mind which allowed me to explore my topic and the research process. Thanks to Dr Simon Guest for his prior work on many of the subjects touched upon in this project, and for his patience in many discussions of symmetry. Thanks to Tim Watson for constant discussion and encouragement throughout the project; you are a great friend. Thanks to Martin Walker for discussions on linkages and literature recommendations. Thanks to Professor Zhong You and Professor Joseph Gattas for enlightening comments on 6R linkages and parameterizations. Of course, thanks to my parents for their constant support, ideas and advice. Finally, thanks to the Foreign and Commonwealth Office and the Marshall Aid Commemoration Commission for funding support.



## Abstract

Kirigami design differs from origami by allowing cuts and material removal in addition to folding. This work explores the use of kirigami as a basis for transforming flat sheets into 3D shapes. By formulating the principles of kirigami with topology and differential geometry, a framework is developed for transforming a sheet between flat and curved configurations by “suturing” cuts in a sheet. This framework is demonstrated by designing and analyzing the pure kirigami unit cell. We find that this unit cell is a type of plane symmetric 6R linkage. We analyze the linkage and illustrate two possible tessellations. Planar design suitable for standard subtractive machining processes ensures the manufacturability of the structures. We expect this system to find applications in morphing structures and robotics where transitions between curvature states are desired.



# Table of contents

<b>List of figures</b>	xiii
<b>List of tables</b>	xvii
<b>1 Introduction</b>	1
1.1 Purpose and Background . . . . .	1
1.2 Scope and Aims . . . . .	3
1.3 Outline of Thesis . . . . .	4
<b>2 Background</b>	5
2.1 Literature Review . . . . .	5
2.2 Discussion . . . . .	10
<b>3 Topology and Geometry</b>	13
3.1 Euler Characteristic . . . . .	13
3.2 Gauss-Bonnet Theorem . . . . .	15
3.3 Discrete Gauss Bonnet Theorem . . . . .	16
3.4 Polyhedral Unfolding . . . . .	18
3.5 Curvature of Kirigami Sheets . . . . .	20
<b>4 Structural Mechanisms</b>	23
4.1 Rigidity and Mobility . . . . .	23
4.2 Denavit-Hartenburg Protocol . . . . .	27
<b>5 Squares, Rhombuses and Jellyfish</b>	31
5.1 The Square Lattice . . . . .	31
5.2 The Jellyfish Lattice . . . . .	35
<b>6 The Octopus Cell</b>	41
6.1 Mobility and Symmetry . . . . .	41

6.2	Geometry . . . . .	45
6.3	Linkage Analysis . . . . .	49
6.4	Octopus Networks . . . . .	51
<b>7</b>	<b>Conclusions and Future Work</b>	<b>57</b>
7.1	Conclusions . . . . .	57
7.2	Future Work . . . . .	58
	<b>References</b>	<b>65</b>

# List of figures

1.1	An origami sheet folded using the Miura-ori pattern subjected to a twisting force [1]. . . . .	2
1.2	An example of compliant kirigami, implicated here for solar energy applications [2]. . . . .	3
3.1	A general topological surface with holes in an open and closed configuration. The sheet is two-dimensional, compact, and changes between simply connected (right) and not (left). . . . .	13
3.2	A basic example of how topological invariants such as the Euler characteristic $\chi$ are combined algebraically. . . . .	14
3.3	Thin sheet with a hole in open and closed configurations. This is the most basic building block of a kirigami sheet transforming between two and three dimensions. In the closed configuration, the sheet's external boundary must accommodate the change in genus $g$ of the sheet. . . . .	16
3.4	(a) Non-developable vertex, $v$ , with angle defect, $d(v)$ , positive curvature and facet angles $\mu$ . (b) The spherical map of the vertex. The defect of the vertex is shown as the area, $d(v)$ , of the spherical quadrilateral with interior angles $\rho$ . The facets $A$ and $B$ map to vertices on the spherical polygon. . . . .	17
3.5	Statement of the general problem. (a) A single, fictitious kirigami cell in some folded and cut configuration. (b) Given a cutting forest, we seek a flattened kirigami geometry. . . . .	19
4.1	A series of three revolute joints in a general linkage. The arrows show the direction of transformations and the variables involved. . . . .	28

---

4.2	The 6R linkage analog to the kirigami unit cell, shown in its initial planar configuration. Coordinate transformations are made from joint 1 to joint 4 in both directions around the loop to generate a closure condition based on a modified Denavit-Hartenburg protocol. . . . .	29
5.1	The basic square kirigami in plan view with the active cell shaded in red. One rigid pyramidal truss unit is shown separately. . . . .	32
5.2	The three primitive unit cells with active cells shown in red. All configurations are made by tessellating these actuated cells. (a) shows a “peak” cell, (b) a saddle cell, (c) a “bowl” cell. The peak and bowl cells impart positive Gaussian curvature due to a positive angle defect while the saddle imparts negative Gaussian curvature due to its angle surplus. Each primitive is shown in an intermediate actuation state, with a single deformed square subunit becoming rhombic. . . . .	33
5.3	Basic square lattice kirigami. The active cell is shown shaded in red. (a) Flat, unfolded annulus state. (b) Transition state. (c) Sutured disc state with hole fully closed. . . . .	34
5.4	A single cell of the square kirigami in the closed configuration with facets labeled 1-8. (a) The spherical Gauss map of the positive vertex is shown in blue with area $\frac{\pi}{2}$ . (b) The negative vertex in green with area $\pi$ . (c) The total internal map in red for $\rho = \frac{\pi}{2}$ (d) The total internal map for a general value of $\rho$ . The total internal map has zero area. . .	35
5.5	The square lattice with shaded squares indicating actuator placement. (a) A square tessellation with inserted rows and columns of rigid squares. This configuration leaves one degree of freedom for single curvature in one of two directions. (b) The stiff configuration for the square kirigami sheet. In this mode, the second degree of freedom in the unit cell is constrained by the rows above and below and can only exist in this non-developable state. . . . .	36
5.6	Rhomboidal kirigami sheet with active cells shown in red. This is an example of a lattice using point-wise connections which we avoid due to increased freedoms, complexity, and manufacturing difficulty. We focus on kirigami lattices that can be feasibly manufactured using edge-wise connections. . . . .	36
5.7	(a) The flattened jellyfish. (b) A partially folded configuration. (c) The geometric parameters of the jellyfish. . . . .	38

---

5.8 (a) The regular jellyfish lattice bending in multiple directions due to twisting compliance of the trapezoidal panels. The magnitude of this twist is on the order of $\psi$ , the curvature along each axis on the jellyfish cell shown in the superimposed Gauss map. (b) A side view of the tessellation without compliance. $\psi$ is the curvature along each axis and $t$ is the thickness of the corrugation in the fully closed state defined in Eqn (5.8). . . . .	39
5.9 A jellyfish cell manufactured from HDPE plastic. . . . .	39
6.1 (a) Geometric parameterization of a one degree-of-freedom kirigami unit cell in its planar state. Vectors labeled $k$ are fold lines; those labeled $d$ are hole edges. (b) Rendering of the unit cell in a partially folded configuration. The origin (of the coordinates shown in red) is placed in the same position as in the parametric analysis. . . . .	42
6.2 The contact polyhedra, $C$ , for symmetry calculations. (a) $C$ for the doubly symmetric linkage. (b) $C$ for the singly symmetric linkage. . . . .	42
6.3 Paper prototype showing three mobility modes of the octopus cell. (a) Primary symmetric mode. (b) Secondary symmetric mode. (c) Antisymmetric mode. . . . .	43
6.4 Open and closed states of the unit cell from Fig. 6.1. (a) The open, planar configuration shows the unique interior and exterior vertex angles. (b) The closed configuration shows the contours used to produce Gauss maps. The green and blue contours yield the positive and negative Gauss maps for individual vertices, respectively, while the red contour yields the gauss map of the interior of the unit cell in its closed configuration. These maps are shown in Figs 6.5 and 6.6, respectively. . . . .	45
6.5 (a) One of two angular defect vertices in the interior of the closed until cell and its corresponding Gauss map. (b) The center saddle vertex of the closed unit cell and its corresponding Gauss map. . . . .	45
6.6 Gauss map of the three interior vertices in the closed configuration of the unit cell. The total solid angle as a sum of each signed area is zero; thus, the interior holds no net Gaussian curvature as expected. . . . .	46
6.7 Side and front view of the unit cell with parametric values shown. . . . .	47
6.8 Three views of the three-dimensional isosurface shown in blue, which provides all continuous solutions given a geometric quantity $\beta$ for the linkage as a function of $\rho_1$ and $\rho_2$ . Contours on the surface are shown in red. . . . .	51

6.9 (a) For a one dimensional tessellation with $n$ units, we have $2^n$ configurations, with five shown. By adjusting the geometry of the unit, we can create tessellations in a range of shapes. (b) Rendering of one configuration. (c) Physical prototype. . . . .	52
6.10 A possible tessellation in two dimensions. All units are closed in the same sense here, approximating a doubly curved sheet. The tessellation uses two unique unit cells shown in red and blue, with hinge lines rotated by $\frac{\pi}{2}$ . (a) Side view of the tessellation. (b) Isometric view with the unfolded configuration. (c) Physical model. . . . .	52
6.11 (a) Design for an 8 cell octopus ring. (b) Design for a 16 cell octopus ring. (c) 8 cell physical prototype. (d) 16 cell physical prototype. . . . .	53
6.12 (a) Top view of the cell in the open configuration. (b) Side view of the cell in the closed configuration. (c) Top view of the cell in the closed configuration. . . . .	53
6.13 Paper prototype of an singly-symmetric octopus cell. (a) The open configurations. (b) The mode due to geometric hinge alignment, without compliance. (c) The closed, antisymmetric mode requiring facet compliance. . . . .	54
6.14 (a) A hexagonal octopus cell with unequal side lengths and only one symmetry plane. (b) A hexagonal unit cell with two symmetry planes. .	54
6.15 Design for a 2D tessellation of equal-sided hexagonal cells. (a) The flat-folded state. (b) Unfurled to the planar state. (c) The partial closed folded state. (d) The final, non-developable closed cylinder state. . . . .	55
6.16 A 1D tessellation of singly-symmetric hexagonal cells. This cell can be used to create conical forms. . . . .	55
7.1 An interactive design tool for the jellyfish geometry rendered fast in the browser using the open-source JavaScript library Three.js. . . . .	59
7.2 A polygonal facet containing two hinge lines with geometric values labeled.	61

# List of tables

4.1	The general layout of a character table. . . . .	25
4.2	The six classifications of the Bricard linkage and their parameter relationships, derived by J.E. Baker [3]. . . . .	30
6.1	The $C_s$ character table. . . . .	43
6.2	The symmetry calculation for the symmetric octopus cell. . . . .	43
6.3	The symmetry calculation for the asymmetric octopus cell. . . . .	44
6.4	Denavit-Hartenberg parameters for the general 6R kirigami linkage. . .	49



# Chapter 1

## Introduction

You admit there are many holes in that piece of cheese... In other words, holes exist. But holes are not made of matter; to the contrary, they result from the absence of matter.

---

*Stephanie & David Lewis  
Holes, 1970*

### 1.1 Purpose and Background

Natural structures adapt to environmental changes: many mammals shed their coats and regrow them according to the seasons; many mollusks have shells that grow over time with their bodies; plants change the shape of their leaves depending on their moisture content and access to sunlight. Our built environment provides a stark contrast; while the world around us is constantly changing, most of our architecture and devices are static. This discrepancy calls for structures that can change and adapt to a dynamic environment.

One of the chief reasons that structures are static is the structural design methodology. Static structures are, for the most part, simpler to design than their dynamic counterparts, and thus are more attractive when used in safety-critical scenarios. However, allowing designs to move beyond linear limits opens an exciting door for the possibilities of what can be created.

One exciting technological prospect is the merging of digital and analog engineering into what is called the Internet of Things (IoT) [4]. While still on the horizon, the

concept of an IoT includes feedback loops for all objects— a network of information both digital and physical. Extreme geometries will prove fruitful for developing such physical structures capable of reacting to digital and physical signals from other objects. As technology progresses, morphing structures will play a crucial role in providing the technical means of creating multipurpose inventions capable of adaptation and reaction.

Most manufacturing processes begin in two dimensions due to simplicity in design, machining, and material handling. Thus, we begin with the concept of a physical map between two and three dimensions—what can we design in two dimensions that is capable of being transformed into three dimensions? How much information can be encoded in a flat sheet of material to produce a nontrivial, three-dimensional structure? Intuitively, we can imagine a multi-piece design framework where many, separate, flat objects connect to form a single structure. However, if we constrain our design methodology to retain the connectedness of the original sheet we can circumvent the added complexity associated with assembly rules [5].

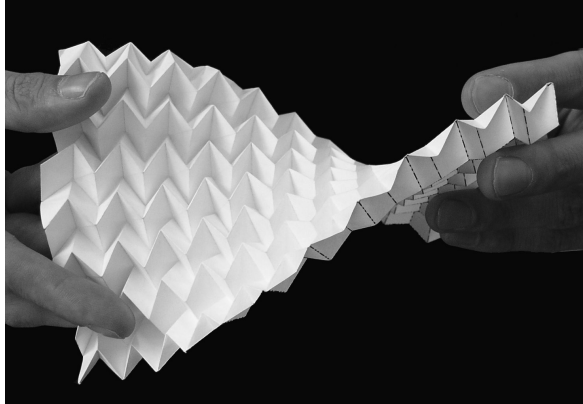


Fig. 1.1 An origami sheet folded using the Miura-ori pattern subjected to a twisting force [1].

One of the oldest forms of manufacturing from flat sheets of material is origami, from the Japanese words for fold, *ori*, and paper, *gami*. This process relies on prescribing fold lines in a sheet to create a three-dimensional shape. Kirigami, from the Japanese word *kiri* meaning “to cut”, is a form of origami which has seen recent attention as an extension of the folding practice. While origami has drawbacks such as excess material and intricate folds, kirigami techniques circumvent these difficulties by allowing for the removal of excess material and the production of objects with simpler folds. In both cases, information is programmed into sheets through the geometry of folds and,

in the case of kirigami, cuts. The principles underpinning these kirigami cuts are an active topic of research, and many open questions remain, such as generalized cutting rules that will allow embedding of the sheet in three dimensions [6].

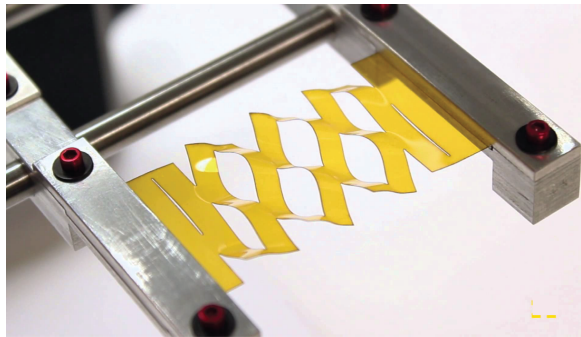


Fig. 1.2 An example of compliant kirigami, implicated here for solar energy applications [2].

## 1.2 Scope and Aims

This work is motivated by the increasing demand for responsive architectures—interactive objects that respond to their environment. We explore kirigami as a modular framework for transformable surface design. We feel that the fundamental notion of “gluing” a hole in a sheet has not been explored properly in an engineering setting. Thus, we begin with the concept of a hole, and explain why changing the number of holes is something of a metaphysical magic trick. We move on to the physical implications of holes and frame the discussion within a structural engineering context to explore the fecundity of the concept. Our goal is to formulate a vocabulary to analyze sheets with holes to facilitate the prototyping of morphing kirigami design.

We focus on the analysis of unit cells with several geometries, and describe the ability to tessellate these cells into repeating structures. We attempt to assemble the foundations of kirigami from topological principles to its geometric implications by combining concepts from several fields of study, placing kirigami engineering in the context it demands. We envision a reconfigurable surface composed of kirigami units that is able to change between a variety of global shapes. We hope for this work to elucidate the principles of morphing kirigami design and to demonstrate kirigami as a means of developing shape-changing structures towards a variety of applications.

### 1.3 Outline of Thesis

This study is an introduction to kirigami engineering that attempts to remain rooted in fundamental concepts and realized through several designs. Kirigami has garnered much attention in the past decade across a variety of fields including mechanism theory and geometry. In Chapter 2, we provide a concise literature review to place our work in the context of these fields and others connected to kirigami research. We offer a brief discussion in Section 2.2.

Closely bordering on the philosophical, topological concepts are introduced to explore the implications of hole-cutting and subsequent hole-gluing within in a flat sheet of material. From topology, we gain specificity by transitioning to topological embeddings in three-dimensional Euclidean space. After an introduction to polyhedral curvature, we examine the concept of “unfolding” as it pertains to kirigami. These topics are discussed in Chapter 3.

A large branch of civil and mechanical engineering deals with the kinematics of mechanisms. We find that kirigami objects can be modeled using concepts and techniques from mechanism theory. This toolkit is introduced in Chapter 4. We begin a specific analysis of kirigami using two regular cell types, the square and rhombus cells, and one irregular variant dubbed the *jellyfish* cell named for its curved shape. We discuss tiling rules for these cells and their geometric constraints in Chapter 5. By analyzing the square and rhomboidal lattices, we are able to design a geometry that can provide a general path to creating arbitrary shapes from kirigami sheets. We dub this novel unit cell the *octopus* based on its organic aesthetic and motion. The design and its possible tessellations are analyzed in Chapter 6. A concluding discussion is offered, followed by an outline of important future steps in Chapter 7.

# Chapter 2

## Background

### 2.1 Literature Review

We begin our background discussion with a brief survey of contemporary research in origami, kirigami, and their related fields. We aim to provide a context for this work by finding open questions in the field and describing methods by which they can be explored. Our goal is to develop a novel research direction for the design and analysis of morphing structures stemming from kirigami. The design of such structures is rooted in the discovery and analysis of repeating unit cell constructions.

The key to understanding how kirigami unit cells and their tessellations behave is understanding the intrinsic geometry of the cells, linking spherical geometry to discrete origami vertices composed of planar facets [7]. Recently, a revisit to the basic origami was undergone to classify all degree-four vertices based on their sector angles [8]. Linear algebraic tools based on orthogonal transformations are often used to model rigid origami [9]. Extending this analytic work, simulation software has been developed to design complex origami and simulate its folding motion [10, 11]. These numerical techniques generalize several well-known origami patterns to create an infinite number of user-defined shapes with various qualities such as developability, and the tool is conveniently packaged into an open-source software package. One drawback of this software is that it is primarily based on the Miura-Ori pattern, and still requires form-finding on the part of the user. We often see the Miura-Ori pattern used as a starting point for folded structure design. The mechanical properties of the classical Miura tessellation under load have been studied [12, 13]. Extensions of the repeating Miura pattern to create singly-curved structures have been analytically parameterized and fabricated for both developable and non-developable patterns [14]. Recent research uses a vertex approach to design arbitrary Miura cross sections by parameterizing

intersecting planes of vertex coordinates, though doubly curved structures are not defined, and the starting geometry is limited [15]. Similarly, analytical treatments have been extended using nonlinear optimization techniques to approximate a given target surface with a locally altered Miura-Ori pattern. Naturally, doubly-curved structures using this technique are non-developable, and few are rigid foldable [16]. Thus, there have been extensive efforts to parameterize and numerically solve for patterns stemming from the Miura-Ori design, though these geometries still prove limited and double curvature is rare. Much of these models abstract the origami problem far beyond physicality, such that we find ideas from paper folding infiltrating abstract concepts of mathematics and physics.

For example, deformations of polyhedral surfaces can be insightful for research in pure mathematics, where results for polyhedral surfaces have a link to integrable systems [17]. In physics, the topic of “topological mechanics” is of recent interest, which includes the examination of defects in the Miura pattern as an analogous problem in the field of condensed matter [18]. Origami can be made into a lattice theory problem, exchanging creases and vertices in a fold pattern for edges and nodes in a graph [19]. Removing facets from large fold patterns can be analogous to topological insulators through a concept called “topological polarization” [20]. When discussing Gaussian curvature in the context of polyhedral sheets, the concept of phyllotaxis is closely related. Phyllotaxis uses the concept of the Euler characteristic to explain the interplay between 5, 6, and 7-sided Voronoi cells in tiling circular domains, while providing a method for explaining the curvature induced by a topological shift on a polyhedral lattice such as the spiral patterns of a sunflower’s seeds [21]. These endeavors are far removed from structural design, but are insightful in their illustration of the fundamental role origami can play in understanding nature. Starting with the modeling origami, our investigative reach is far.

The design and analysis of mechanical linkages is a more closely related area of research. Linkages are essential to the study of deployable and morphing structures, beginning with trellis-type structures using generalized scissor mechanisms for the design of deployable rings [22]. Origami models have inspired the study of symmetric 6R linkages and linkage combinations [23]. For example, a 5R linkage can be created by combining two 4R linkages, and in a similar fashion, two of these 5R linkages can combine to create a 6R linkage that is apt for a deployable net showing similarities to deployable origami model [24]. Other notable examples include the threefold symmetric Bricard linkages and the networked Bennett linkages designed using geometric compatibility [25, 26]. Origami and linkages are closely related through their mathematical

models, and analogies between origami and linkages have been made for a variety of crease patterns [27]. Despite the inspiration from origami in the realm of linkages, there is little reciprocation. Most geometries of folded structures continue to revolve around the Miura pattern.

However, there has been recent progress in the drastic alteration of the Miura design. By combining unit cells with different geometric scales to form “zig-zag” sheets, a structure is created that exhibits a single degree of freedom sheets including rhombus holes [28, 29]. This kirigami-inspired technique can be used to tune the mechanical properties of the Miura sheet and its variants by changing the design’s geometry while retaining the finite mechanism. This advancement is still limited to the constraints imposed by the Miura geometry, and is simply a variant. Similarly, by beginning with a Miura pattern, removing certain facets and slightly misaligning the hinge lines, a single degree of freedom sheet is shown to naturally deploy based on stored potential energy due to geometric frustration [30]. This methodology might provide a solution for low-energy deployable structures. However, the design relies on pin-joints which may prove difficult to physically realize. Structures designed using a combination of different geometries have been constructed for a range of origami and kirigami patterns as well [31]. Many of these design, however, rely on the assembly of many individual components which removes the deployable character of the original origami.

The Miura pattern can also be made in a closed loop fashion, known as the Tachi-Miura polyhedron (TMP) [32]. TMP tubes can be combined in a “zipper” fashion to create one degree of freedom “metamaterials” with tunable stiffness properties [33]. Based on the Miura pattern, tubes have been developed with reconfigurable cross sections with various configurations. Many, but not all, of these tubes are flat foldable, and can deploy along nonlinear trajectories with one degree of freedom per cross-sectional configuration [34]. In three dimensions, tubes can be combined to form a solid, cellular material structure with interesting mechanical properties [35]. This work could inspire three dimensional kirigami design, where voids are programmed in three dimension to tune a structure’s properties.

The work mentioned so far deals exclusively with straight-line crease geometries, though curved creases have been discussed since origami became an engineering endeavor [36]. Algorithms for form-finding and approximation of curved folded structures have been studied and implemented using planar quadrilateral approximations in software [37]. The mechanics of curved creased structures has been explored to investigate the “concentric circles” problem, where creases are made in a circular pattern resulting in a globally curved geometry [38]. Curved crease geometries have been parameterized and

adapted using discretization for use with Miura-type patterns using planar quadrilateral mesh fitting [39]. All of the research mentioned thus far, including curved creasing, assumes infinitesimal thickness of the sheets with localized deformations at the hinge lines, but recent work explores the differences that thickness makes for origami design [40]. While we believe these “unorthodox” design methods are interesting, this study is limited to straight fold lines.

The designs previously discussed are primarily static or with one mode of deformation. There is great interest in the engineering of active structures that can morph in a variety of ways. One goal of this research is to produce arbitrarily curved surfaces from the flat sheets. The kagome lattice has been designed and analyzed for use as an actuated plate structure. Unless the curvature of the target shape is small, however, significant stretching forces will develop and the energy required for actuation will be large [41]. This is a consistent result in the design of activated trusses where energy scales with deformation. Many circumvent this constraint by using elastomeric materials. Such self-assembling sheets using magnetics were developed to create closed polyhedra from elastomer laminates [42]. Using a synthesis of geometry, control algorithms, and materials design, impressive programmable origami sheets have been developed which change shape through active folds. The structures can fold into a variety of shapes from a single fold pattern [43]. The use of actuation at the folds is a common theme, imparting motion to a structure at the site of localized deformation. Hinge-based actuation methods for smart materials applications have been explored using laminate techniques with mixed materials [44]. Many of these concepts have been studied and experimented with, but the vast majority are limited by function rather than by form [45]. The use of pneumatics is a popular method of activating designs. Shape-changing structures have been designed using pressure differentials for shape-changing doubly curved shells, and origami designs using elastomers have been explored to create pneumatically controlled transformable shapes [46, 47]. This methodology couples bending and stretching to create curved structures with a range of curvatures. A promising 3D unit cell utilizing embedded pneumatic actuation to produce multiple lattice configurations has been developed to create a novel framework for creating morphing spatial lattices from regular polyhedra [48]. There are difficulties with pneumatic actuation, however, such as leaks, positional accuracy and manufacture. Origami-inspired designs using unit cell actuators to achieve multistability are prevalent as well. Bistable concepts that employ bending and twisting to transform between stable configurations have been developed based from biological inspiration [49]. Nested rhombuses using piezoelectric ceramics have been designed with some success [50].

When combined, tape springs can serve as bistable actuators to create a multistable structure [51]. Multistable plate structures using a series of bistable elements has also been designed by combining corrugated and compliant sheet structures [52]. This arrangement has  $n$  configurations for  $n$  actuators rather than a continuous deformation as seen in the pneumatic structures.

The problem of injecting curvature into sheets has been studied from a continuous perspective as well. PDMS bilayers programmed with curvature using a lithography process were designed to produce Gaussian curvature as the result of local compression, inducing out of plane buckling [53]. Swelling in thin sheets to produce buckling has been solved analytically for a small number of shapes using energy methods [54]. These techniques are out of reach for rigid folding, but the goal of this work is the same: to understand how curvature can be created. For thin sheets, some work has been done on curvature dipoles modeled using a ridge and two conical surfaces. For example, the mechanics of shell deformation when curvature is “injected” has been derived using geometry and energy methods [55]. A computational study for these crumpling-type problems has been done as well to uncover power law relationships between bending, stretching and self-avoidance [56]. An interesting geometric singularity found in this work on crumpling is the developable cone, which has been explored analytically using energy and geometric methods [57, 58]. We see that this curvature-based research involves bending and stretching of thin sheets, whereas the chief tenet thus far of engineering origami is the rigid facet assumption.

Rigid kirigami maintains this assumption and attempts to produce embedded curvature. Kirigami cuts and folds on regular lattices have been developed using a constrained set of rules [6]. So-called “pluripotent” materials produce out-of-plane geometries from kirigami, where the distribution of cuts made in a sheet are limited to a hexagonal graph and its triangular dual [59]. Experiments show approximate curvature through the use of basic kirigami building blocks. The result is a mapping from a target surface to the kirigami structure where the achievable gradient is limited by the size of the chosen unit cell. This work does not exhibit a sheet with true double curvature as it implies, but an approximation of a target surface using stepwise geometry. Other lattices have been parameterized in a similar fashion, including the “cube” and “eggbox” kirigami geometries. These are used to design space frames based on the edges of the facets [60]. The cellular honeycomb kirigami concept is a promising direction for lightweight curved structures that uses a combination of cutting and folding to create hexagonal core sheets through a gluing process [61]. This technique has spawned much research in adaptations and characterizations of the kirigami honeycomb, including

patterns for general cross-sections with single curvature [62]. The pluripotent and honeycomb structures might be called “orthodox” as they do not permit compliant facets.

Some unorthodox endeavors combine elastomers with kirigami cutting. For example, stretchable electronics have been studied and mechanically characterized, though these structures rely solely on the elasticity of the substrate, and not on a fold pattern [63]. The concept of cutting planar sheets to create stretchable batteries has been implemented with some success [64]. Using micro and nanoscale pre-strain techniques with patterned cuts, an array of shapes can be created using the spirit of kirigami designs [65, 66]. A promising direction for this unorthodox kirigami work is the promise of dynamic kirigami structures which utilize both patterned cuts and elastic deformations for solar tracking applications [2].

## 2.2 Discussion

The wealth of research combining origami, linkages, kirigami and geometry is connected by the goal of creating and analyzing lightweight structures that incorporate folds, cuts and patterned geometries. Several themes emerge in the prior work. First, the global effects of local changes plays an important role in the design of morphing materials. A unit cell is designed and analyzed first to understand both its unique characteristics and the global effect of its transformation. In our work, it seems logical to design a unit cell first, and then understand its possibilities for tiling. Second, the prior research of transformable sheets includes the constraint of planar facets and the allowance of bending in sheets, each problem having its own drawbacks. The rigid facet assumption makes modeling more straightforward, but less interesting global shapes are typically produced. However, bending and stretching is an energy intensive process that is not available for most engineering materials. This work will explore this dichotomy in more detail. Third, a common goal in this field is to produce curvature from non-curved objects. While cuts and holes have been used to create materials with interesting properties, we intend to explore the use of voids in a material as the key design element.

Rather than base designs on existing patterns, we begin with the concept of the hole and explore the consequences of its existence and the transformations this phenomenon can induce. Focusing on an analytical approach, we work towards an elegant design scheme with clearly defined, yet broad, constraints. One issue recognized in the prior work is geometric form-finding, which leads to many derivative designs. Rather than deriving, we aim is to freely invent and subsequently analyze our findings to reach

conclusions about the possibilities of what can be created. We seek novel structures through the implementation of holes; thus, we must begin with a fundamental question: what is a hole?



# Chapter 3

## Topology and Geometry

### 3.1 Euler Characteristic

Sometimes referred to as “rubber sheet geometry”, the subject of topology is a necessary mathematical starting point for a fundamental understanding of the kirigami problem, for topology is the study of holes. If we begin by quelling specific shapes and thicknesses of materials to focus on the chief function of kirigami, to open and close holes, we can better understand how to extend our thinking into the creation of engineering objects. Thus, we begin by thinking in terms of homeomorphisms— changes in shape of

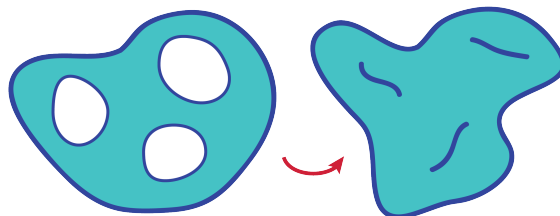


Fig. 3.1 A general topological surface with holes in an open and closed configuration. The sheet is two-dimensional, compact, and changes between simply connected (right) and not (left).

an object by stretching without tearing. We can think of topological objects as being composed of faces, edges, and vertices. A face must be simply connected, meaning it is a contractible space such that no contour within the face may surround a hole. In other words, all faces are homeomorphic to a point. Additionally, a finite edge can exist only between two vertices without self-connection. We introduce the Euler characteristic to classify such objects topologically. The Euler characteristic,  $\chi$ , of a polyhedral surface

is defined as [67]

$$\chi = V - E + F \quad (3.1)$$

where  $V$ ,  $E$  and  $F$  are the number of vertices, edges, and faces respectively. Note that  $\chi$  does not tell us the dimension of space in which an object is embedded or other attributes of the object such as orientability or compactness:  $\chi$  is a topological invariant, and, more specifically, a “homotopy invariant”. Topological objects can be arranged into groups of homotopic equivalence, where objects have equal Euler characteristics. While homeomorphic surfaces have the same Euler characteristic, the converse is false [68]. We can explore a basic algebra if we imagine calculating  $\chi$  for various simple objects as shown in Fig. 3.2. Since  $\chi$  is 1 for a disc and  $\chi$  is 0 for an

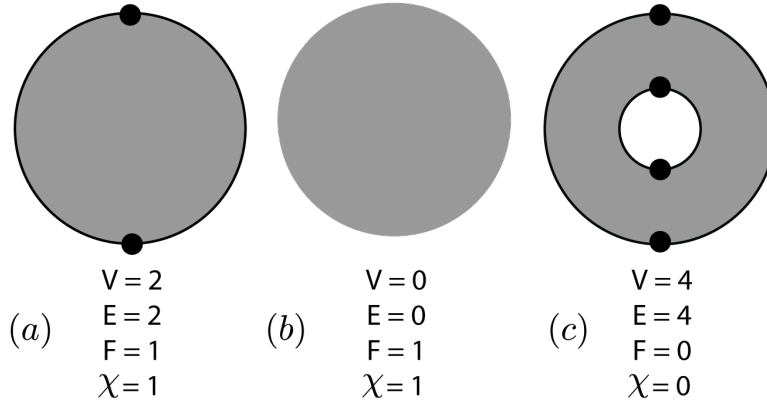


Fig. 3.2 A basic example of how topological invariants such as the Euler characteristic  $\chi$  are combined algebraically.

annulus (a disc with a single hole), we see that the combination of two objects can be computed algebraically. For example, a circle has  $\chi = 0$  as there are the same number of vertices as edges, making the addition of a circle and a disc equal to 1 as shown in Fig. 3.2. We can subtract a disc from a disk to form an annulus with  $\chi = 0$ . For higher order topologies, the combinatorial approach is extended algebraically: a disc with  $g$  holes is the subtraction of  $g$  discs from an original, simply connected disc. For each additional hole,  $\chi$  is decreased by 1 for the sheet, which can be proven by induction. Thus, a perforated sheet has a characteristic

$$\chi_{\text{sheet}} = \chi_{\text{disc}} - g(\chi_{\text{disc}}) = 1 - g \quad (3.2)$$

where  $g$  is the number of perforations and  $\chi_{\text{disc}}$  is 1: this is a direct analog to closed orientable objects, objects with a definitive *inside* and *outside*, without topological

twists, of genus  $g$ . For three-dimensional, orientable objects, genus describes the number of handles. For example, a coffee cup is, topologically, a single toroid as it has a single handle:  $g$  is 1.  $\chi_{\text{toroid}}$  is  $2 - 2g$  such that  $\chi_{\text{sheet}}$  is  $\frac{1}{2}\chi_{\text{toroid}}$  [67]. This basic topological analysis is enlightening for the design of a kirigami surface. Closing a kirigami hole changes that object's homotopy group. By designing cuts strategically within a sheet, we may be able to change the geometry of that sheet by closing cuts. Thus, we seek a building block to create a global shape— a repeating kirigami unit to transform the sheet between homotopy groups. By programming the geometry of each unit, we can create an array of global shapes when individual units are combined.

## 3.2 Gauss-Bonnet Theorem

Topological principles, however, are not concerned with physical materials: “rubber-sheet geometry” is just that— abstractions of objects in any dimension without resistance to large in-plane deformations. In order to move one rung down the ladder of abstraction, we seek a connection between the three-dimensional geometry of perforated sheets and their topology. This link is given by the Gauss-Bonnet Theorem, stated as

$$\int_S K \, dA + \int_{\delta S} k_g \, ds = 2\pi\chi. \quad (3.3)$$

$K$  is the Gaussian curvature within the surface,  $S$ , and  $k_g$  is the geodesic curvature integrated over line elements,  $ds$ , along the boundary,  $\delta S$ , of  $S$  [67]. This curvature computation is equated to the topological invariant  $\chi$  from Eqn (3.1). This form of the theorem applies to orientable, compact objects— conditions our kirigami structures must obey. This is an astounding result in differential geometry, a commandment for how objects must obey their topological invariant whilst undergoing deformation. A fundamental intuition of Gaussian curvature is essential for understanding the importance of morphing kirigami structures. Rather than merely changing the shape of an object, we can completely change its structural properties. For the perforated disc from Fig. 3.2, we can insert Eqn (3.2) into Eqn (3.3) to yield

$$\int_S K \, dA + \int_{\delta S} k_g \, ds = 2\pi(1 - g). \quad (3.4)$$

Thus, we have a relationship between the number of kirigami cuts in our general surface, and how the curvature along the boundaries and within the sheet must reflect the

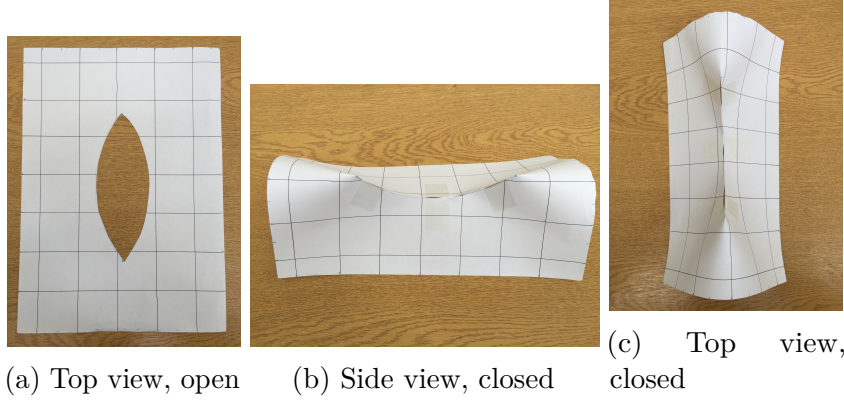


Fig. 3.3 Thin sheet with a hole in open and closed configurations. This is the most basic building block of a kirigami sheet transforming between two and three dimensions. In the closed configuration, the sheet's external boundary must accommodate the change in genus  $g$  of the sheet.

homotopic change when a hole is closed. For brevity, we can rewrite Eqn (3.4) as

$$\tau + \gamma = 2\pi(1 - g) \quad (3.5)$$

for use in subsequent discussion. For a closed surface without boundary,  $\gamma$  will remain exactly 0. For a kirigami cell each hole will add an additional boundary, and the material will always contain an external boundary with changing geodesic curvature to reflect the opening or closing of holes as shown in Fig. 3.3. Thus, changing  $g$  will manifest itself in a change in  $\tau$  and  $\gamma$ .

### 3.3 Discrete Gauss Bonnet Theorem

In this study, we focus on objects that can be modeled as polyhedral sheets with rigid, planar facets. To better understand the shape of general kirigami structures, we can develop a discrete form of Eqn (3.4) which is more efficient in computing the discrete curvature of polyhedral vertices. In its discrete form, we use angle measures and sums as opposed to integrals. We prove their equivalence and show in detail how they are used. For a discrete polyhedral surface,  $S$ , with boundary  $\delta S$  composed of  $n$  geodesics each of curvature  $k_g$ , it is straightforward to show

$$\sum_{i=1}^n \int_{\delta S_i} k_g \, ds = 0 \quad (3.6)$$

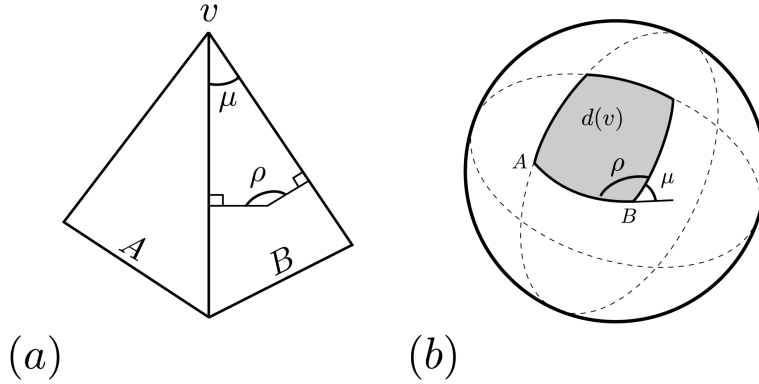


Fig. 3.4 (a) Non-developable vertex,  $v$ , with angle defect,  $d(v)$ , positive curvature and facet angles  $\mu$ . (b) The spherical map of the vertex. The defect of the vertex is shown as the area,  $d(v)$ , of the spherical quadrilateral with interior angles  $\rho$ . The facets  $A$  and  $B$  map to vertices on the spherical polygon.

for each boundary edge  $\delta S_i$ . These edges are straight line segments (edges) with geodesic curvature 0. The boundary curvature is defined by the turning, or exterior, angles at the edge vertices,  $\mu_{ext}$ , where

$$\mu_{ext}(v) = \pi - \sum_i \mu_i \quad (3.7)$$

for each  $v \in \delta S$  where  $i$  facets converge. The Gauss-Bonnet Theorem for a polyhedral surface composed of planar facets can be rewritten as

$$\int_{\delta A} K dA + \sum_{v \in \delta S} \mu_{ext}(v) = 2\pi(1 - g). \quad (3.8)$$

It can be shown that the Gaussian curvature concentrated at an interior polyhedral vertex  $v$  is exactly  $d$ , the angle defect of that vertex [69]. Since we restrict all facets to be rigid and planar for our kirigami, the integral of the Gaussian curvature over the surface is equal to the sum of the interior angle defects and each vertex defect is equal to the solid angle,  $A$ , subtended by a Gaussian spherical map of that vertex where

$$A = (2 - n)\pi + \sum_{i=1}^n \rho_i. \quad (3.9)$$

$\rho_i$  is the interior angle of the  $i^{th}$  vertex of the spherical  $n$ -gon. It is trivial to show that  $\mu_i$ , the interior angle of the  $i^{th}$  facet at polyhedral vertex  $v$ , is equivalent to  $\pi - \rho_i$  making the angle defect,  $d$ , of that vertex

$$d(v) = 2\pi - \sum_{i=1}^n \mu_i. \quad (3.10)$$

The Gauss-Bonnet Theorem can thus be rewritten in discrete form as

$$\sum_{v \in S_{int}} d(v) + \sum_{v \in \delta S} \mu_{ext}(v) = 2\pi(1 - g) \quad (3.11)$$

for a polyhedral surface,  $S$ , with interior  $S_{int}$  and boundary  $\delta S$ . The parameters used in this derivation are shown in Fig. 3.4. A similar analysis has been employed in computational geometry as a straightforward method of calculating discrete curvature for a polyhedral mesh [70]. We use this framework to explore the curvature of our kirigami unit cell. By constructing a series of Gauss maps, it becomes clear how the curvature of the surface changes throughout its transformation, and provides insight for how kirigami cells might be tessellated to form a globally curved shape. An important definition to state here is “developable”, in terms of a surface. A developable polyhedral surface contains no vertices with nonzero discrete Gaussian curvature. To flatten a non-developable surface, some tear or cut must be made within the surface. Note that a fold is developable, and thus a vertex through which a single fold passes has exactly zero curvature.

## 3.4 Polyhedral Unfolding

We define *pure kirigami* as the removal of material within the boundary of a finite sheet, and note that we subsequently use the term *kirigami* to mean this construction. What, then, are the limits of kirigami? While fold lines are prescribed within the sheet to allow for mobility, what collection of non-developable vertices can be created to produce a globally curved kirigami structure? This problem falls under a niche category of origami engineering known as polyhedral unfolding, a graph theory topic in disguise. We investigate several key results in that field to mathematically define kirigami and build a vocabulary to better understand the geometric constraints involved.

A graph is a collection of edges and vertices; a path is an ordered traversal of vertices on a graph through its edges; a cycle is a path that returns to its starting point. A tree is a graph with no cycles, and a forest is a disjoint collection of trees.

Removing a single edge from a tree results in a forest. A cutting graph, or cutting, is a collection of edges on a simply connected polyhedral surface or closed polyhedron that separates faces of that surface or polyhedron. We seek cuttings that result in connected, flattened polyhedral surfaces called unfoldings. Specifically, we require unfoldings to not contain overlaps. Given a polyhedral surface, we can show that any unfolding is a forest, and that the cutting must traverse all vertices with nonzero curvature. By contradiction, if the cutting has a cycle, the unfolding will be disjoint. We want to retain the connectedness of our polyhedron in order to manufacture shapes from single sheets. Of course every polyhedral sheet has a trivial cycle along its boundary vertices, thus we exclude this case. If the cutting in question did not traverse all vertices with nonzero curvature, the faces joined by these vertices would not be flattenable. Thus, every nonzero curvature vertex must be included in the cutting.

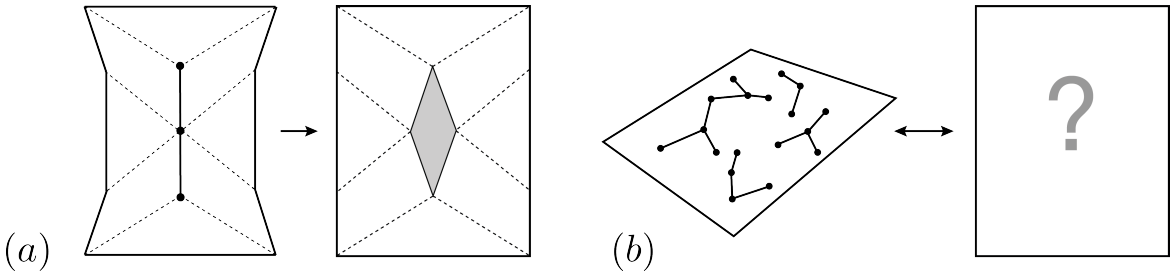


Fig. 3.5 Statement of the general problem. (a) A single, fictitious kirigami cell in some folded and cut configuration. (b) Given a cutting forest, we seek a flattened kirigami geometry.

The flattened polyhedral surface need not be simply connected, thus the cutting need not be a tree. As shown in Fig. 3.5, a pure kirigami cell is a counterexample for this assumption. It is through connections of this type of component that we wish to create a global kirigami structure unfolded by a cutting forest. It has been proven that the requirement for this construction is nonconvexity [71]. We digress here to briefly define convexity with effort to do justice to the field of convex polytopes.

*A set  $K$  of  $\mathbb{R}^n$  is convex if, for each pair of distinct points  $a, b$  in  $K$ , the closed segment with endpoints  $a$  and  $b$  is contained within  $K$  [72].*

Another measure of nonconvexity is the existence of “saddle corners”, or vertices of negative discrete Gaussian curvature [73]. Convex polytopes do not contain saddle negative curvature vertices.

Thus, for a closed, convex polyhedron, we know that, generally, the cutting must be a forest, and the connected graph condition of the cutting stems from the convexity

condition. Assuming the cutting were a forest, one can imagine a closed contour on the polyhedron's surface, across its faces, that encloses one of the forest's trees entirely, avoiding any and all vertices of the polyhedron. When the cutting is made, this contour must unfold and flatten with the polyhedron meaning the sum of its turning angle,  $\tau$  from Eqn (3.5), must equal  $2\pi$ . From the closed condition, the left-hand side of Eqn (3.5) must be  $2\pi$ . Due to the convexity condition,  $\gamma$  must be greater than or equal to zero (in the flattened state). However, since the contour must enclose at least one vertex of the polyhedron and the convexity condition enforces positive curvature on these vertices,  $\tau$  must be strictly greater than zero. Since  $\gamma$  must be less than  $2\pi$  to comply with Eqn (3.5), the polyhedron cannot flatten. Thus, the cutting of a convex polyhedron must be a tree. Note that every negative curvature vertex must be connected to two cut edges, as a single cut would allow the faces of that vertex to overlap by its angle surplus. With these definitions and propositions defined, we apply this manner of thinking to explore what is possible for pure kirigami constructions.

### 3.5 Curvature of Kirigami Sheets

We would like to create kirigami structures with nonzero global curvature, an open polyhedron with some net angle defect, for double curvature is useful in creating shell structures with high strength to weight ratio such as spherical caps and saddles. This leads us to a question: does a polyhedral surface of some nonzero global curvature have a cutting that does not include any boundary vertices? In essence, we seek the existence of a non-developable structure with a cutting forest. We impose neither the convexity nor the closed condition on this structure, only that it has some nonzero net Gaussian curvature, no overlaps in the flattened state, and a disjoint cut tree. These are the requirements of a kirigami sheet in the language of graphs. We seek a flat sheet that can transform into a polyhedral shell or saddle by hole closures.

A pure kirigami object, by our definition, is a polyhedral sheet with a cutting forest that does not include any boundary vertices. For a kirigami object with net nonzero Gaussian curvature, every interior vertex would need to have nonzero curvature. Thus, every vertex would need to be traversed by a cutting forest. For the pure kirigami unit, we use the simplest hole, the rhombus cut, as shown in Fig. 3.5(a). This unit creates three vertices, one of negative curvature and two of positive curvature. As the hole is closed, the curvature of the internal boundary in the flat configuration must shift to the outer boundary in the closed configuration. In order to create a global sheet through the addition of these kirigami units, the boundary vertices of

adjacent cells are connected. In order to retain the disjoint cutting, the boundary vertices must combine to form vertices with zero curvature. Since every interior vertex in a doubly-curved surface must have nonzero curvature vertices, this construction contradicts the constraints imposed by the disjoint cutting forest. In order to create doubly-curved kirigami, the boundary vertices of the sheet must be contained by the cutting or the sheet will not be developable. Stated formally, all bounded polyhedral surfaces with disjoint cut trees which disassemble their non-developable vertices have net-zero global curvature. Thus, pure kirigami can not be used to construct bounded polyhedral surfaces with double curvature. This does not mean that we cannot create singly curved or ruled surfaces using pure kirigami, which provides a rich design space. We explore this space in detail in Chapter 5 and Chapter 6.



# Chapter 4

## Structural Mechanisms

Our kirigami concept has thus far been abstracted into a polyhedral surface with planar facets. We would like to tune the mobility of our kirigami such that we can design its topology and geometry for a variety of applications. By thinking of our polyhedral sheet as a pin-jointed bar framework, we can better understand the mobility and rigidity of our structure using the language of truss kinematics. Exploring counting rules for rigidity and mobility is a starting point for classifying our sheet structures.

### 4.1 Rigidity and Mobility

We have shown that polyhedral sheets can be understood topologically through an invariant called the Euler characteristic. However, this value does not directly quantify the rigidity of that structure. Counting rules emerged to understand the rigidity of trusses, and are still a topic of research today. Maxwell is credited with the earliest rigidity formula

$$b = 3j - 6 \quad (4.1)$$

where  $j$  is the number of joints and  $b$  the number of bars in a structure free to move as a “rigid” body in three dimensional space. This early relationship was extended through an analysis of the matrix of frame structures [74]. By investigating the general structures of the equilibrium and compatibility matrices for pin-jointed frames, it can be shown that these two matrices are related through their rank and nullspace. This knowledge can be related to the number of states of self-stress  $s$  and mechanisms  $m$  of the structure in question. The extended Maxwell-Calladine rule is

$$b - 3j + 6 = s - m. \quad (4.2)$$

Note that given two structures with equal numbers of bars and joints, this rule yields the relationship between  $s$  and  $m$ , but it takes a full matrix analysis or inspection to investigate the exact numbers of these phenomena. In addition, this counting of self-stresses and mechanisms does not entail a description of their existence. This is left to inspection or experiment. In kirigami engineering, we can apply these rules in a similar fashion as we would for pin-jointed frames, simply by adopting the conventions of the latter. This calculation is shown in detail in Chapter 5.

A mechanical linkage is a series of rigid bodies joined by a series of mechanisms which allow certain relative freedoms between bodies. Lower kinematic pairs are mechanisms which allow freedoms between two bodies such that both connected bodies move in the same fashion. We restrict our analysis to one type of lower pair—revolute joints, as we are dealing only with fold lines. Revolute joints allow a single rotational freedom between bodies. A sheet of pure kirigami is a collection of rigid bodies connected through revolute joints. Our goal is to better understand if and how these bodies move relative to one another in space, and the geometric details of their movement. A counting rule of note for linkages is the Grübler-Kutzbach criterion, based on the number of freedoms removed by a kinematic pair

$$m - s = 6(b - 1 - j) + \sum_{i=1}^j f_i. \quad (4.3)$$

where  $m$  is the mobility, or number of freedoms of the structure,  $s$  is the number of self-stresses,  $b$  is the number of bodies, or links, of the linkage,  $j$  is the number of joints, and  $f_i$  is the number of freedoms allowed by joint  $i$  [75]. For a kirigami structure,  $f_i$  will always equal 1 since every kinematic pair is a revolute joint. Thus we can rewrite the formula as

$$m - s = 6(b - 1) - 5j \quad (4.4)$$

for a kirigami structure unconstrained in three dimensions. For closed-loop linkages  $b = j$ , making the mobility criterion

$$m - s = j - 6. \quad (4.5)$$

Thus, the rule predicts that a closed kinematic chain of less than or equal to six bodies will be immobile, an overconstrained linkage. These linkages are well-studied, and many are in fact mobile under precise geometric conditions. The case of  $j = 6$  is discussed in subsection 4.2.1.

### 4.1.1 Symmetry

For kinematic loops of  $j < 6$ , we can extend Maxwell's and Grubler's rules for the geometric mechanisms found in these curious closed chains. Work from the kinematics of molecules has crossed over into the structural mechanics realm to provide answers. Much of these answers use the language of the representation theory of finite groups, which we will briefly summarize here. A group, in this realm, is a collection of isometries in Euclidean space, specifically the collection of orthogonal transformations. The orthogonal group  $O(n)$ , in three dimensions, comprises the group of rotations and reflections centered around a point  $n$ . This group can be represented through matrices, and the group operation is thus matrix multiplication. A representation is a description of a group through a linear transformation, and can be reducible or irreducible. To find the mechanisms of a structure due to symmetry, we seek to describe the freedoms and constraints imposed by the bodies and their joints in terms of irreducible representations. In essence, the act of rotating a revolute joint is a linear transformation which can be represented within  $O(n)$ , and it is with this representation that we can determine how symmetry plays a role in the freedoms of a structure made up of these linear transformations. A character, in the representation of finite groups, is the trace of a group element in question, here a matrix trace. Thus, for a given rotation or reflection, the character is the trace of that particular transformation matrix [76]. Molecular symmetry has led to the convenient organization of all of these elements into character tables for various point groups, groups of isometries that keep one point fixed. A general table is shown in Table 4.1. For a "natural" coordinate system, one

Table 4.1 The general layout of a character table.

Point Group in Schöenflies Notation	Conjugacy Classes of Operations in the Group
Mulliken Symbols for Irreducible Representations	Characters

that in the realm of structural mechanisms corresponds to the edges of the mechanism, the transformation matrices are simply permutation matrices that change the position of graph vertices and edges. For every element that is unchanged after a symmetry operation, a 1 is left on the diagonal of the matrix representation for that operation making the character the trace of this matrix, the number of unchanged elements. This way, we can calculate the characters of the symmetry representation as the character

of the irreducible representation from a character table multiplied by the number of nodes or bars unchanged by this operation. Character tables can be found in standard molecular symmetry texts [77]. By translating our vocabulary for understanding the rigidity of frames, we can show that the criterion for rigidity from Section 4.1 must become

$$\Gamma(b) - \{\Gamma(j) \times \Gamma_T - \Gamma_T - \Gamma_R\} = \Gamma(s) - \Gamma(m) \quad (4.6)$$

where  $\Gamma(b)$  and  $\Gamma(j)$  are the representations of the bars and joints,  $\Gamma_T$  and  $\Gamma_R$  are the representations of the rigid body translations and rotations which depend on the point group in question, and  $\Gamma(s)$  and  $\Gamma(m)$  are the representations of the self-stresses and mechanisms. It is seen that this is a stronger condition that relies on the irreducible representations of different point group symmetries to establish the relationship between  $s$  and  $m$ . In the realm of structural analysis, this condition does not provide as much information as a full matrix analysis of a structure, but it does establish a more specific rigidity criterion that takes symmetry into account. We can develop a similar intuition for polyhedral surfaces by finding the dual of the polyhedral to form what is termed the contact polyhedron,  $C$  [75]. This replaces the pin jointed structure described by Eqn (4.3) with a graphical object where the facets of the surface become nodes and the hinges become directed edges to determine the effects of symmetry operations. A mobility condition for polyhedral surfaces with revolute joints can be written as

$$\begin{aligned} \Gamma(m) - \Gamma(s) = & \Gamma(v, C) \times \{\Gamma_T + \Gamma_R\} \\ & - \Gamma_{\parallel}(e, C) \times \{\Gamma_T + \Gamma_R\} \\ & - \{\Gamma_T + \Gamma_R\} + \Gamma_f \end{aligned} \quad (4.7)$$

where  $\Gamma(v, C)$  and  $\Gamma_{\parallel}(e, C)$  are representations of the permutation of vertices and edge vectors in the contact polyhedron, analogues to  $\Gamma(j)$  and  $\Gamma(b)$  in Eqn (4.6).  $\Gamma_f$  is the representation of freedoms allowed by the joints in the linkage. To calculate  $\Gamma_f$  we must compute  $\chi_{R_r}(S)$ , the character of the rotation around the joint line  $r$  for the connected rigid bodies, and  $\chi_{e_{\parallel}}(S)$ , the character of the contact polyhedron edge  $e$  both undergoing symmetry operation  $S$ . These values are linked by

$$\chi_{\text{revolute}}(S) = \chi_{R_r}(S)\chi_{e_{\parallel}}(S) \quad (4.8)$$

to yield the character  $\chi_{\text{revolute}}(S)$  of each revolute joint undergoing symmetry operation  $S$ .  $\chi_{\text{revolute}}(S)$  is then summed over every unchanged joint undergoing  $S$  to find  $\Gamma_f$ . A full proof of this relationship is given by Guest [75]. We can see that this rule has

the same structure as Eqn (4.3), with the same logic of counting the freedoms of rigid bodies, subtracting the constraints imposed by rigid joints, and adding the necessary freedoms allow by those joints back to the structure. Eqn (4.7) will be explicitly calculated in Section 6.1 for the general 6R linkage.

## 4.2 Denavit-Hartenburg Protocol

Given a group of rigid bodies connected by kinematic lower pair mechanisms, we can establish coordinate systems at each of the bodies according to specific protocol. The standard protocol developed by Denavit and Hartenberg and used by others for origami mathematics demands placing one orthogonal unit vector along a hinge line and another along an adjacent face [78]. By transforming each coordinate system to the next, we can build equations for the position of any point along the kinematic chain. In the case of kinematic loops, this analysis can create loop closure conditions for structure. These equations can be used to calculate the angles of each facet relative to its neighbor, and are useful in explore the mode shapes of a kirigami object. The Denavit-Hartenberg approach creates a standard set of variables for placing coordinate frames, and also for organizing kinematic variables involved in the transformations. the transformations are affine, orthogonal transformations normally carried out using matrix multiplication. The steps for transforming coordinate systems are shown below and a figure of a partial kinematic chain is shown labeled with the parameters in Fig. 4.1.

1. rotate  $z_{i-1}$  around  $x_{i-1}$  by  $\alpha_{i-1}$  to find  $z_i$
2. translate  $O_{i-1}$  along  $x_{i-1}$  by  $a_{i-1}$
3. rotate  $x_{i-1}$  around  $z_i$  by  $\theta_i$  to find  $x_i$
4. translate  $O_i$  along  $z_i$  by  $d_i$

The transformation matrix from link  $i$  to  $j$  in terms of these parameters is

$$T_{ij} = \begin{bmatrix} \cos \theta_i & -\sin \theta_i & 0 & a_i \\ \cos \alpha_i \sin \theta_i & \cos \theta_i \cos \alpha_i & -\sin \alpha_i & -d_i \sin \alpha_i \\ \sin \alpha_i \sin \theta_i & \cos \theta_i \sin \alpha_i & \cos \alpha_i & d_i \cos \alpha_i \\ 0 & 0 & 0 & 1 \end{bmatrix} \quad (4.9)$$

This protocol is primarily a numerical technique as the output equations for loop closure or end effector position tend to be large and nonlinear. Analytical expressions

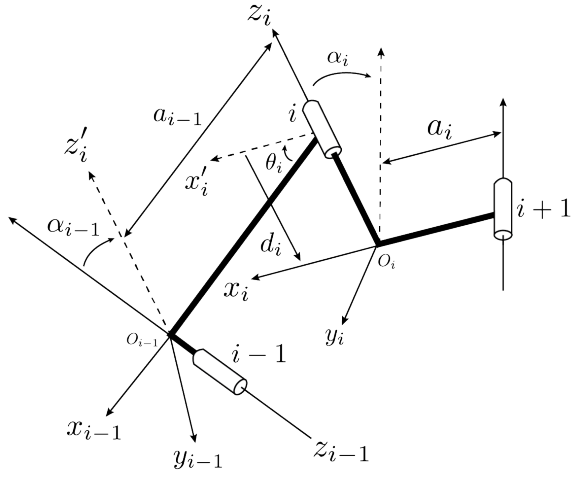


Fig. 4.1 A series of three revolute joints in a general linkage. The arrows show the direction of transformations and the variables involved.

are difficult to find as the equations often have many solutions. In some cases symmetry can be exploited to produce a set of manageable equations. This is explored further in Chapter 6.

### 4.2.1 6R Linkages

The 6R linkage loop is interesting because it contains the maximum number of joints and links of any overconstrained linkage according to Eqn (4.3). The linkage must contain the same number of mechanisms as self-stresses by simple counting of its constituent parts or contain some symmetric mobility modes. Linkage loops can be created by combining shorter loops, such as multiple 4R Bennett linkages attached in parallel. When a 6R linkage is not created by combining other overconstrained linkages but exists in a unique geometric form it is known as a Bricard linkage. Bricard linkages are geometrically mobile due to symmetries, and Baker calculated the governing equations for the six symmetry classifications of Bricard linkages [3]. These are listed in Table 4.2 for reference. The translational parameters,  $a$  and  $d$ , and the rotational skew parameter,  $\alpha$ , as shown in Fig. 4.2 are listed with their constraints for each Bricard type. According to these constraints, we can prescribe the geometry of the linkage by supplying 18 values. This leaves 6 kinematic parameters,  $\theta$ . Constraints on these parameters are listed in the table. With this information, we can use the

loop closure equations generated by the Denavit-Hartenberg protocol and algebraic manipulation to produce input-output relationships for a specific linkage's angles in a given configuration. We seek to compare the parameter constraints for kirigami mechanisms with these Bricard linkages to find similarities which will aid in networking such linkages and give insight into the geometric character of kirigami.

We have seen how structural mechanism theory is useful for organizing linkage topologies into groups and analyzing their kinematics in a systematic manner. Combining this vocabulary with topology and geometry, we are ready to embark on an exploration of kirigami unit cells. We begin with the simplest unit cell, a kirigami formed from the square lattice.

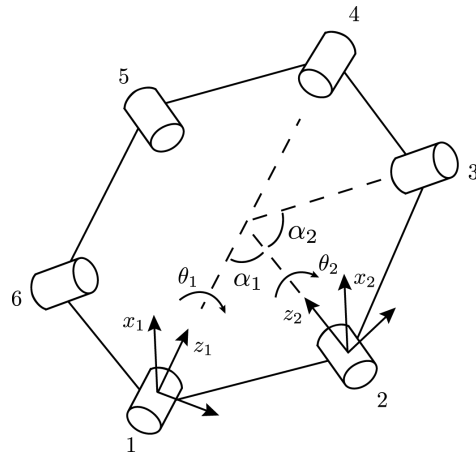


Fig. 4.2 The 6R linkage analog to the kirigami unit cell, shown in its initial planar configuration. Coordinate transformations are made from joint 1 to joint 4 in both directions around the loop to generate a closure condition based on a modified Denavit-Hartenburg protocol.

Table 4.2 The six classifications of the Bricard linkage and their parameter relationships, derived by J.E. Baker [3].

Type of Symmetry	Twist Angle ( $\alpha$ )	Link Length ( $a$ )	Turn Angle ( $\theta$ )	Offset Length ( $d$ )	Notes
General Line Symmetric	$\alpha_{12} = \alpha_{45}$ $\alpha_{23} = \alpha_{56}$ $\alpha_{34} = \alpha_{61}$	$a_{12} = a_{45}$ $a_{23} = a_{56}$ $a_{34} = a_{61}$	$\theta_1 = \theta_4$ $\theta_2 = \theta_5$ $\theta_3 = \theta_6$	$d_1 = d_4$ $d_2 = d_5$ $d_3 = d_6$	Projection of the linkage reveals its line symmetry. See Section 6.1 for a thorough treatment.
General Plane Symmetric	$\alpha_{61} + \alpha_{12} = \pi$ $\alpha_{56} + \alpha_{23} = \pi$ $\alpha_{45} + \alpha_{34} = \pi$	$a_{61} = a_{12}$ $a_{56} = a_{23}$ $a_{45} = a_{34}$	$\theta_6 + \theta_2 = 2\pi$ $\theta_5 + \theta_3 = 2\pi$	$d_1 = d_4 = 0$ $d_2 = d_6$ $d_5 = d_3$	Joint axes 1 and 4 lie in the symmetry plane.
Trihedral	$\alpha_{12} = \alpha_{34} = \alpha_{56} = \frac{\pi}{2}$ $\alpha_{23} = \alpha_{45} = \alpha_{61} = \frac{3\pi}{2}$	$a_{12}^2 + a_{34}^2 + a_{56}^2 = a_{23}^2 + a_{45}^2 + a_{61}^2$	$\sin \theta_3(a_{61} + a_{12} \cos \theta_1) = \sin \theta_1(a_{34} + a_{23} \cos \theta_3)$ $\sin \theta_5(a_{23} + a_{12} \cos \theta_3) = \sin \theta_1(a_{56} + a_{45} \cos \theta_5)$ $\sin \theta_4(a_{12} + a_{12} \cos \theta_2) = \sin \theta_1(a_{45} + a_{34} \cos \theta_4)$ $\sin \theta_6(a_{34} + a_{12} \cos \theta_4) = \sin \theta_1(a_{61} + a_{56} \cos \theta_6)$ $\sin \theta_2 \sin \theta_3 = \sin \theta_5 \sin \theta_6$	$d_i = 0$ for all $i$	The relationships for $\theta_i$ are defined geometrically. The six local coordinate origins define a hexahedron. The quadrilateral faces determine the angle relationships.
Line Symmetric Octahedral	$\alpha_{12} = \alpha_{45}$ $\alpha_{23} = \alpha_{56}$ $\alpha_{34} = \alpha_{61}$	$a_{i,i+1} = 0$ for all $i$	$\theta_1 + \theta_4 = 2\pi$ $\theta_2 + \theta_5 = 2\pi$ $\theta_3 + \theta_6 = 2\pi$	$d_1 + d_2 = d_3 + d_4 = d_5 + d_6 = 0$	The sign convention for alternating $d$ values is changed to simplify the model. This is a special case of the line-symmetric 6R.
Plane Symmetric Octahedral	$\alpha_{12} = \alpha_{45}$ $\alpha_{23} = \alpha_{56}$ $\alpha_{34} = \alpha_{61}$	$a_{i,i+1} = 0$ for all $i$	$\theta_1 + \theta_4 = 2\pi$	$d_1 = -d_4$ $d_2 = -d_1 \frac{\sin \alpha_{34}}{\sin \alpha_{12} + \alpha_{34}}$ $d_3 = d_1 \frac{\sin \alpha_{12}}{\sin \alpha_{12} + \alpha_{34}}$ $d_5 = d_1 \frac{\sin \alpha_{61}}{\sin \alpha_{45} + \alpha_{61}}$ $d_6 = -d_1 \frac{\sin \alpha_{45}}{\sin \alpha_{45} + \alpha_{61}}$	This linkage is not actually plane symmetric.
Doubly Collapsible Octahedral	$\alpha_{12} = \alpha_{45}$ $\alpha_{23} = \alpha_{56}$ $\alpha_{34} = \alpha_{61}$	$a_{i,i+1} = 0$ for all $i$	$\theta_1 + \theta_4 = 2\pi$ $\theta_2 + \theta_5 = 2\pi$ $\theta_3 + \theta_6 = 2\pi$	$d_1 d_3 d_5 + d_2 d_4 d_6 = 0$	This linkage involves a trigonometric intermediate step to find the offset relationship.

# Chapter 5

## Squares, Rhombuses and Jellyfish

Cutting a disc from a thin sheet and joining the edges of the hole together produces a minimal surface containing a saddle and two peaks [55]. Discretizing the disc into a rhombus results in the simplest hole that can be completely closed along straight edges. Thus we begin with the simplest 4-vertex lattice as a starting point for our kirigami cells. We provide an explanation of the units from a kinematic and curvature perspective, and discuss possible tilings of the cells.

### 5.1 The Square Lattice

We begin the design of our kirigami sheets with quadrilaterals due to their fundamental simplicity and rigidity. It is straightforward to prove that there are only three regular tilings of the Euclidean plane: the triangle, the square, and the hexagon. Were we to choose a lattice of vertex degree three, the hexagonal lattice, we would expect exactly zero mechanisms while degree six would offer mechanisms within each repeating unit hexagon. For a repeating lattice of degree four, the square lattice, we can expect a minimal number of mechanisms. Thus, the square lattice allows us to focus on the geometric action of hole glueing using the most straightforward geometry. For this reason, it is a starting point for our kirigami unit cell subject to modification. The square lattice offers an annulus with a hole the same shape as the rigid facets surrounding it, meaning it is the simplest instantiation of the pure kirigami we seek to characterize.

### 5.1.1 Mobility

We first generate equations describing its mechanisms according to Section 4.1. We convert a single quadrilateral facet into a bar-and-joint structure in three dimensions by removing the mechanisms found in a four-bar. We add four more bars out of plane to create a square pyramid, and remove the mechanism in the base by adding a cross bar. This 3D truss analogue is shown in Fig. 5.1. For a tessellation of  $p$  rows and  $q$

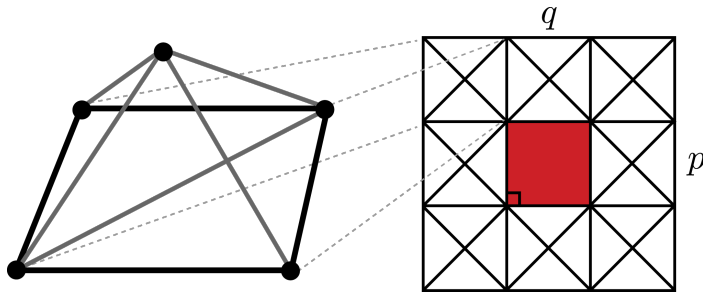


Fig. 5.1 The basic square kirigami in plan view with the active cell shaded in red. One rigid pyramidal truss unit is shown separately.

columns, we can count the number of bars

$$b = 7pq + p + q \quad (5.1)$$

and the number of joints

$$j = 2pq + p + q + 1. \quad (5.2)$$

We can substitute this into Section 4.1 to find a relationship for the mechanisms  $m$  and self-stresses  $s$

$$s - m = pq - 2p - 2q + 3. \quad (5.3)$$

Based on inspection, we know that each facet has no self-stresses or redundancies, and  $m$  is 0 as expected when  $p$  and  $q$  are 1. For four facets in a 2x2 tiling  $m = 1$ , and for a 3x3 tiling  $m = 0$  which the formula incorrectly predicts due to symmetry. By inspection, we see that a 3x3 tiling has at most two mechanisms either in the vertical or horizontal directions. This is true in general for a quadrilateral sheet with geometrically aligned hinges: the number of mechanisms is  $p - 1$  or  $q - 1$  depending on the direction of the hinge lines being altered. By activating the center square of a 3x3 tiling to form the square kirigami as shown in Fig. 5.1, we find  $m = 2$ , the correct number of mechanisms for a structure of this bar and joint count. We imagine this center square as an actuator to give the structure mobility. This measure is corroborated

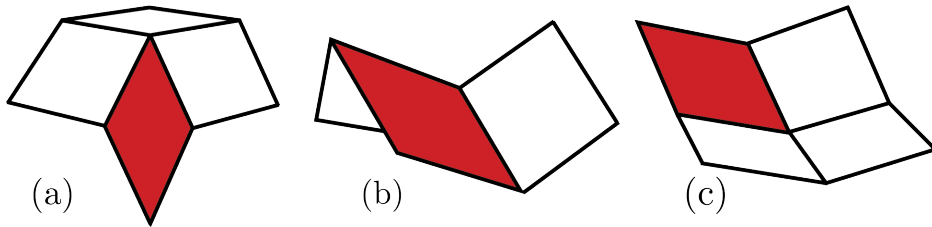


Fig. 5.2 The three primitive unit cells with active cells shown in red. All configurations are made by tessellating these actuated cells. (a) shows a “peak” cell, (b) a saddle cell, (c) a “bowl” cell. The peak and bowl cells impart positive Gaussian curvature due to a positive angle defect while the saddle imparts negative Gaussian curvature due to its angle surplus. Each primitive is shown in an intermediate actuation state, with a single deformed square subunit becoming rhombic.

by Eqn (4.3), where we use the dual of the square grid to find the mechanisms of an 8R linkage analogue. Using Eqn (4.5), we find two mechanisms as we would expect. The task is now to understand how these mechanisms are manifested in the structure. In Fig. 5.2, we see how the “active” center cell creates positive or negative Gaussian curvature around the central vertex. When these cells are tessellated, how does the curvature manifest itself, and how is it related to the mechanisms?

### 5.1.2 Curvature

We must take into account the consequences of the chosen topology. Given a finite square lattice, its Euler characteristic is precisely 1, a topological disc. This sets the curvature of the sheet at  $2\pi$  when its configuration is completely closed according to Eqn (3.11). The transition between the annular and closed configurations is shown in Fig. 5.3. The hole is referred to as the “active cell” in anticipation of an actuator controlling the degree of openness of the hole. To have a better sense of the curvature available to the sheet in the square geometry, we turn to spherical Gauss maps. As shown in Fig. 5.4, taking the map of each vertex in the cell’s closed configuration, we find the magnitude of the curvature contained by that vertex. The positive curvature vertices contain  $\frac{\pi}{2}$  and the negative vertex contains  $\pi$ , as we would expect from the angle deficit and excess at each of these vertices. To confirm these findings, we take the Gauss map of all three vertices and find that there is zero subtended area in the map, even in the case of the second degree of freedom. This confirms the inability of the lattice to embed nonzero Gaussian curvature regardless of its geometry. The map contains information about the free dihedral angle due to the single degree of

freedom in the closed state. This might prove to be an interesting insight into the kinematotropy of kirigami linkages [23].

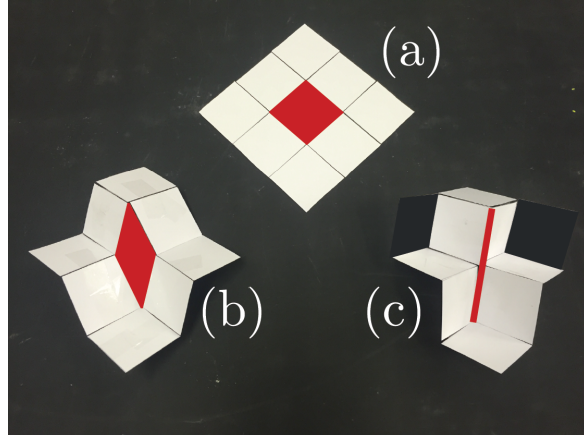


Fig. 5.3 Basic square lattice kirigami. The active cell is shown shaded in red. (a) Flat, unfolded annulus state. (b) Transition state. (c) Sutured disc state with hole fully closed.

### 5.1.3 Square & Rhombus Lattice

Based on the analysis of curvature for the unit cell, we better understand the geometric constraints on the assembly of a square kirigami lattice. The kirigami hole and its gluing count for one degree of freedom in the cell. For the lattice, there are only one configuration in which a lattice can exist for the minimal number of “active” cells. When the active cells are fully deployed with  $\beta = \frac{\pi}{2}$ , the surface converges onto the Escher steps known in recent results as 5-7 climb pairs on a square lattice [6] as shown in Fig. 5.3 or to a square corrugation pattern with mechanisms. These two possibilities for pure kirigami tessellation are shown in subsection 5.1.3. Their rules are as follows:

1. Every 2x2 primitive must contain an active cell, as shown in Fig. 5.2.
2. No two active cells may lie concurrent.
3. No edges of two primitives may lie concurrent.

Each tiled unit of two or more primitive cells must adhere to net zero Gaussian curvature, as shown for the continuous case [55]. As discussed in Section 3.5, this constraint applies to the sheet in its entirety, limiting the global Gaussian curvature to exactly zero. Due to tiling, the gluing of holes in the sheet is one degree of freedom

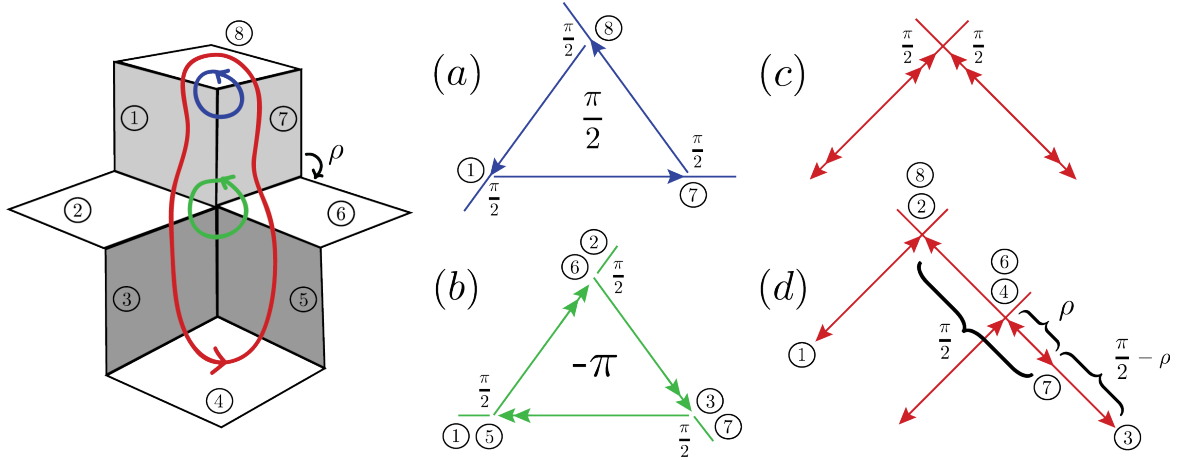


Fig. 5.4 A single cell of the square kirigami in the closed configuration with facets labeled 1-8. (a) The spherical Gauss map of the positive vertex is shown in blue with area  $\frac{\pi}{2}$ . (b) The negative vertex in green with area  $\pi$ . (c) The total internal map in red for  $\rho = \frac{\pi}{2}$  (d) The total internal map for a general value of  $\rho$ . The total internal map has zero area.

regardless of the tessellation size. There still exist other degrees of freedom that are useful to curve the structure in one of two hinge line directions. These rules apply for a rhomboidal lattice as well, where the hinge lines are at an angle that is not  $\frac{\pi}{2}$ . Of course, would need another constraint to fix this freedom, or an actuator to change the angle between the free facets. Note that we are concerned here with lattices connected by hinge lines rather than point connections, as the manufacturability of point connections is low, and the freedoms imparted by point connections are great. To actuate the transformation of such a point-connected structure is not feasible at present. However, interesting tessellations exist in this mode such as the “eggbox” shown in subsection 5.1.3. Notice the greater number of active cells required to create this structure in relation to the square kirigami. The square kirigami geometry can be extended to rectangular cells and alternating rhombus grids as well, while maintaining regularity. We explore the concept of non-regular tessellations in Section 5.2.

## 5.2 The Jellyfish Lattice

We can perturb the square lattice into a non-regular tessellation by shrinking every other square in the tessellation, as shown in Fig. 5.7. This leads to a non-regular tessellation where the unit cell is the same 8R linkage as the square lattice. In a similar

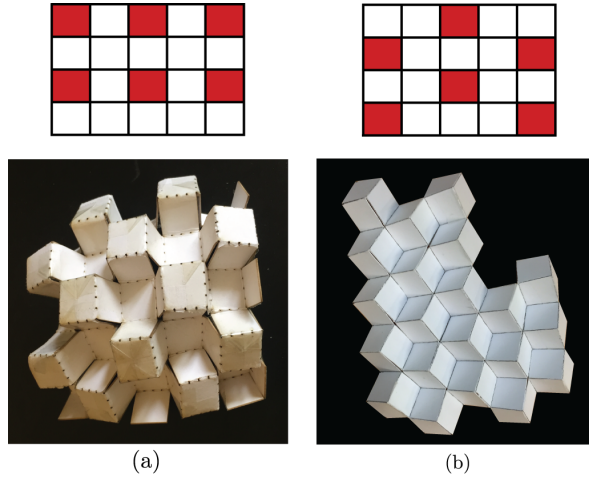


Fig. 5.5 The square lattice with shaded squares indicating actuator placement. (a) A square tessellation with inserted rows and columns of rigid squares. This configuration leaves one degree of freedom for single curvature in one of two directions. (b) The stiff configuration for the square kirigami sheet. In this mode, the second degree of freedom in the unit cell is constrained by the rows above and below and can only exist in this non-developable state.

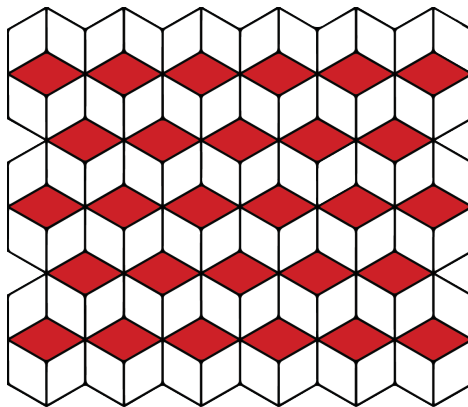


Fig. 5.6 Rhomboidal kirigami sheet with active cells shown in red. This is an example of a lattice using point-wise connections which we avoid due to increased freedoms, complexity, and manufacturing difficulty. We focus on kirigami lattices that can be feasibly manufactured using edge-wise connections.

fashion, we cannot achieve double curvature with this lattice without introducing facet compliance. This agrees with our conjecture in Section 3.5. However, the compliance is locally manifested in the trapezoidal segments of the lattice. This may prove useful, as the lattice could be manufactured using a lithography technique in such a way as to leave these sections of the geometry more flexible than the rigid squares. This is the reason for naming this tessellation the jellyfish; we can imagine its transformative motion similar to the locomotion of the rubbery undersea creature. In the closed, planar configuration without twisting of the trapezoidal facets, we find a relationship for the corrugation thickness for  $t$  defined in Fig. 5.8

$$t = l \cos \phi \sin \theta \quad (5.4)$$

where  $l$  is the edge length of the trapezoid,  $\phi$  is the trapezoid angle and  $\theta$  is the dihedral angle as shown in Fig. 5.7. We can write a relationship between the tessellation geometry and the edge length

$$l = \frac{a - b}{2 \cos \phi} \quad (5.5)$$

such that  $t$  becomes

$$t = \sin(\theta) \left[ \frac{a - b}{2} \right]. \quad (5.6)$$

In the closed configuration we find a relationship between the angle parameters shown in Fig. 5.7

$$\tan \phi = \cos \theta. \quad (5.7)$$

Combining Eqn (5.6) and Eqn (5.7) we find

$$t = \sin \left[ \arccos(\tan \phi) \left( \frac{a - b}{2} \right) \right] \quad (5.8)$$

the thickness of a jellyfish corrugation as a function of its geometric parameters.

We can prove that producing double curvature for the jellyfish sheet must rely on compliance of the trapezoid. Taking normal vectors on each square facet, as shown in Fig. 5.8, we create a Gauss map for a single unit shown in of Fig. 5.7c. It is straightforward to show that the twist,  $\lambda$ , of the trapezoidal facet is on the order of the curvature in each direction,  $\psi$  of the lattice

$$\lambda \sim \psi \quad (5.9)$$

as in the Gauss map in Fig. 5.8. This is confirmed by prototypes, such as the one shown in Fig. 5.9. As an 8R linkage, the jellyfish cell has freedoms to control and utilize during the transformation between flat and multiple closed modes, and multiple modes in the closed state due to geometric alignment of the hinges. We can alter the geometric design of the jellyfish hinges to create conical sections without compliance, though we sacrifice the ability to flat fold the sheets in their original configurations as with the square lattice. In Chapter 6, we explore cells with a single degree of freedom and their promise in creating kirigami sheets.

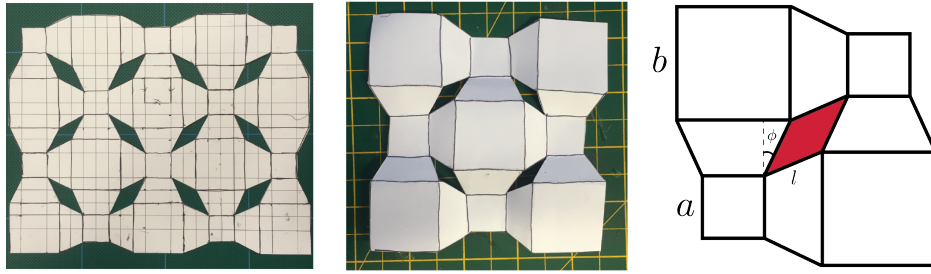


Fig. 5.7 (a) The flattened jellyfish. (b) A partially folded configuration.  
(c) The geometric parameters of the jellyfish.

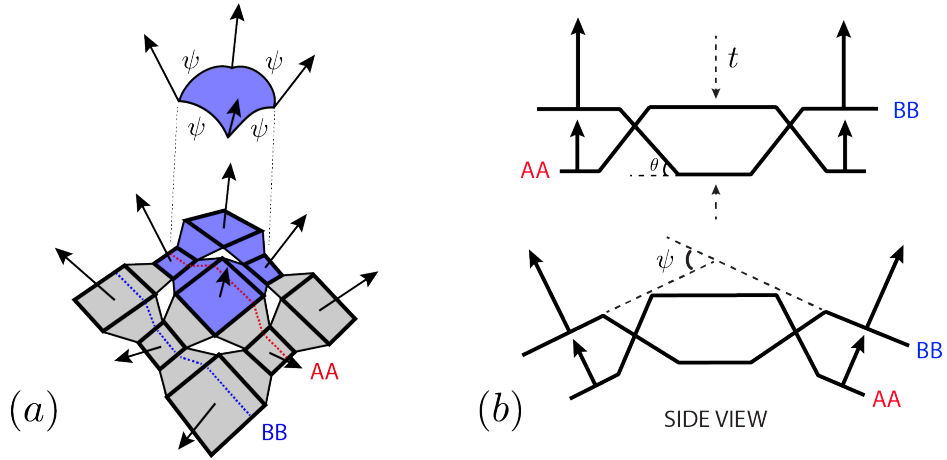


Fig. 5.8 (a) The regular jellyfish lattice bending in multiple directions due to twisting compliance of the trapezoidal panels. The magnitude of this twist is on the order of  $\psi$ , the curvature along each axis on the jellyfish cell shown in the superimposed Gauss map. (b) A side view of the tessellation without compliance.  $\psi$  is the curvature along each axis and  $t$  is the thickness of the corrugation in the fully closed state defined in Eqn (5.8).



Fig. 5.9 A jellyfish cell manufactured from HDPE plastic.



# Chapter 6

## The Octopus Cell

We experimented with unit cells analogous to 8R linkages in Chapter 5. For a sheet with embedded actuators, it is difficult to control two degrees of freedom per unit cell when one of the degrees of freedom is nonplanar. By removing two fold lines, we change the unit cell topology, decrease the degrees of freedom, and create an overconstrained 6R kirigami linkage containing a rhombus hole. We name this cell the “octopus” cell due to its form and motion as shown in Fig. 6.1.

### 6.1 Mobility and Symmetry

We begin an analysis of the octopus cell by investigating its mobility. We identify a special case of the general 6R Bricard linkage analogous to the unit cell drawn in Fig. 4.2. The unit cell is deemed to have equal mobility and states of self-stress with six bodies connected by six single degree of freedom joints. By inspection, the linkage has zero states of self stress and must have zero mobility according to the generalized Kutzbach criterion. However, the linkage has multiple mobility modes due to geometric symmetry. This overconstrained linkage is ideal for the purpose of a morphing sheet because it allows a single actuator to change the shape of a cell while influencing the global shape of the structure. This cell has two symmetry planes; we can create a contact polyhedron  $C$  shown in Fig. 6.2(a) to apply the symmetry-extended mobility formulae described in subsection 4.1.1. By inspection the cell has three folding modes: two symmetric and one antisymmetric shown in Fig. 6.3. We seek these modes through representation calculations. For the doubly symmetric cell, the lowest point group symmetry is  $C_s$ , with one symmetry plane. The character table for this group is supplied in Table 6.1. Using the  $C_s$  character table, we calculate the representations in Table 6.2. The identity operation,  $E$ , does not displace any nodes, thus the difference

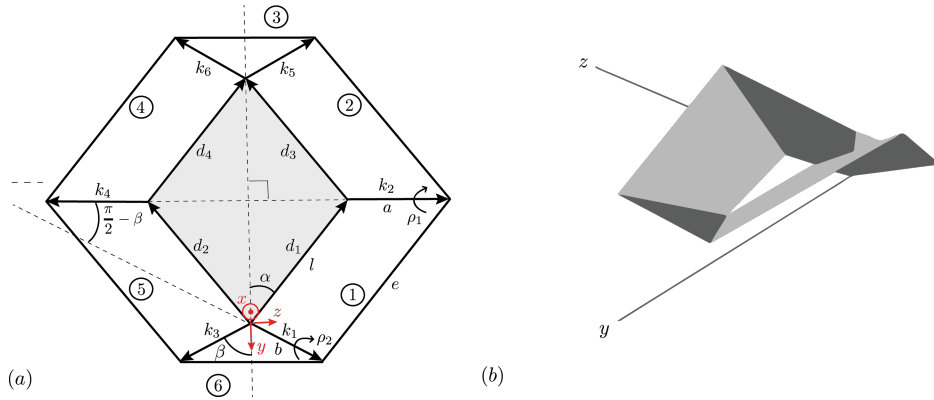


Fig. 6.1 (a) Geometric parameterization of a one degree-of-freedom kirigami unit cell in its planar state. Vectors labeled  $k$  are fold lines; those labeled  $d$  are hole edges. (b) Rendering of the unit cell in a partially folded configuration. The origin (of the coordinates shown in red) is placed in the same position as in the parametric analysis.

between the mechanism and self stress representations is zero, while the symmetry plane provides a difference of two. Since the cell is known to have the same number of mechanisms and self-stresses, due to symmetry there exist two mechanisms and two corresponding self-stresses. From the character table, these mechanisms must belong

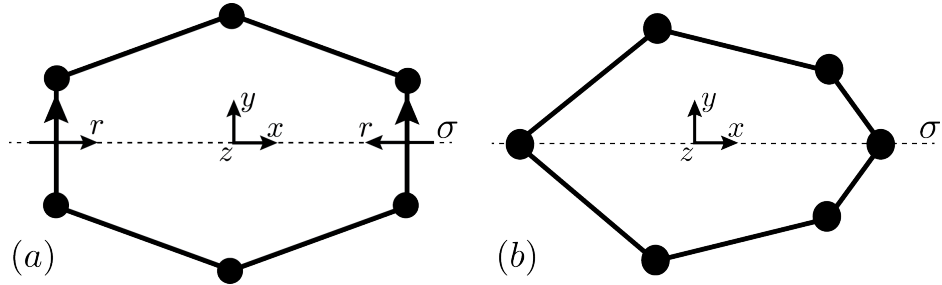


Fig. 6.2 The contact polyhedra,  $C$ , for symmetry calculations. (a)  $C$  for the doubly symmetric linkage. (b)  $C$  for the singly symmetric linkage.

to a symmetric mode,  $A'$ , and an antisymmetric mode,  $A''$ , where

$$\Gamma(m) - \Gamma(s) = A'' - A'. \quad (6.1)$$

Since the representations must be positive, the mechanism here is due to a symmetry and an antisymmetry,  $A' + A''$  and the self stresses are  $A' + A'$ . This means the representation calculation shows one symmetric mechanisms and one antisymmetric,

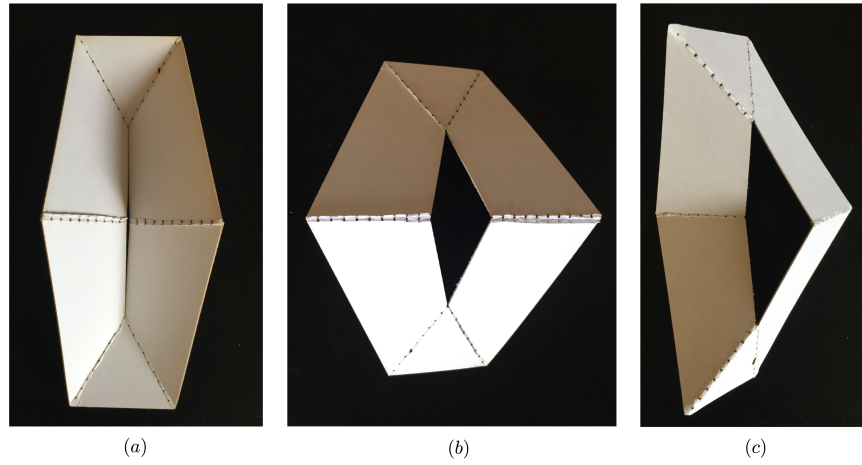


Fig. 6.3 Paper prototype showing three mobility modes of the octopus cell. (a) Primary symmetric mode. (b) Secondary symmetric mode. (c) Antisymmetric mode.

Table 6.1 The  $C_s$  character table.

$C_s$	E	$\sigma$
A'	1	1
A''	1	-1

Table 6.2 The symmetry calculation for the symmetric octopus cell.

$\Gamma(m) - \Gamma(s) =$	E	$\sigma$
$\Gamma(v, C)$	6	0
$\times \Gamma_T + \Gamma_R$	$\times 6$	$\times 0$
$-\Gamma_{\parallel}(e, C)$	-6	$-(-2)$
$\times \Gamma_T + \Gamma_R$	$\times 6$	$\times 0$
$-\Gamma_T + \Gamma_R$	-6	0
$+\Gamma_f$	6	2
=	0	2

with two symmetric self stresses. We can imagine these self stresses being due to hinge misalignment in a translational or rotational sense. This calculation is repeated to explore the mechanisms of the singly-symmetric cell, which is of interest for the design of curved sheets. The contact polyhedron is shown in Fig. 6.2(b). The singly-symmetric cell's plane of symmetry,  $\sigma$ , does not pass through any hinge lines. The representation calculation is shown in Table 6.3 and results in no mechanisms since all hinge lines are permuted by the reflection operation. The resulting representation equation reveals

Table 6.3 The symmetry calculation for the asymmetric octopus cell.

$\Gamma(m) - \Gamma(s) =$	E	$\sigma$
$\Gamma(v, C)$	6	2
$\times \Gamma_T + \Gamma_R$	$\times 6$	$\times 0$
$- \Gamma_{\parallel}(e, C)$	-6	0
$\times \Gamma_T + \Gamma_R$	$\times 6$	$\times 0$
$- \{\Gamma_T + \Gamma_R\}$	-6	0
$+ \Gamma_f$	6	0
=	0	0

$$\Gamma(m) - \Gamma(s) = 0 \times A' + 0 \times A''. \quad (6.2)$$

Thus, there are no symmetric or antisymmetric modes. This is surprising given the ability of the singly symmetric cell to close as shown in Fig. 6.13. Note that the symmetry-extended mobility rule is a necessary but not sufficient condition for mobility, thus there can still exist finite mechanisms in spite of the formula's outcome [76]. In this case, a close inspection of the cell reveals slight compliance in the facets. The magnitude of the necessary compliance to mobilize the singly-symmetric kirigami loop is discussed in subsection 6.2.1. Given the lowest symmetry group,  $C_s$ , for the cell, there is a descent in symmetry between differing planes,  $\sigma$ , which allows for the mobility of the linkage. This fact is useful in the parametric design of repeating lattice structures, as altering the symmetry of neighboring cells has a profound impact on the mobility of the global network. A simple conclusion we can draw from this analysis is to design symmetry through hinge lines to allow mobility. This simple rule could play a powerful role in the design of future kirigami tessellations.

## 6.2 Geometry

To explore the consequences of the fold line removal, we investigate the discrete curvature of the unit cell vertices by applying the discrete Gauss-Bonnet theorem in the open and closed configurations. In the open configuration, summing the interior

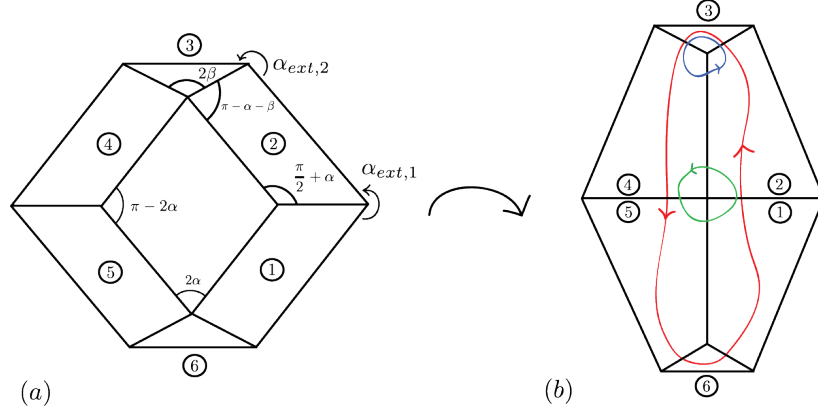


Fig. 6.4 Open and closed states of the unit cell from Fig. 6.1. (a) The open, planar configuration shows the unique interior and exterior vertex angles. (b) The closed configuration shows the contours used to produce Gauss maps. The green and blue contours yield the positive and negative Gauss maps for individual vertices, respectively, while the red contour yields the gauss map of the interior of the unit cell in its closed configuration. These maps are shown in Figs 6.5 and 6.6, respectively.

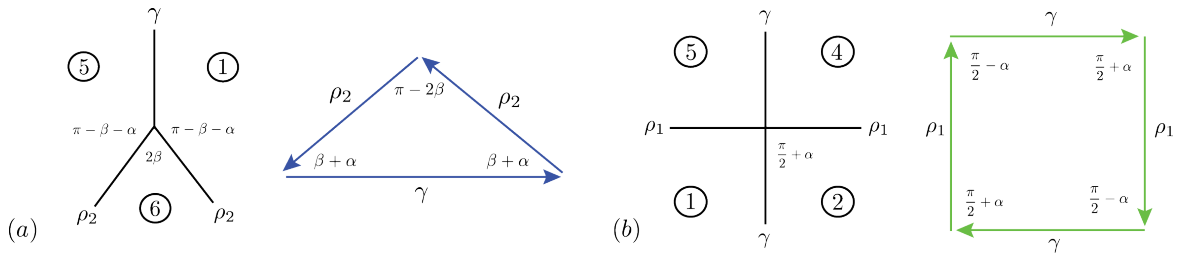


Fig. 6.5 (a) One of two angular defect vertices in the interior of the closed until cell and its corresponding Gauss map. (b) The center saddle vertex of the closed unit cell and its corresponding Gauss map.

rhombus angles and the exterior turning angles of Fig. 6.4 yields

$$[2(2\alpha) + 2(\pi - 2\alpha)] + [4(\pi - \alpha_{ext,2} + 2(\pi - \alpha_{ext,1})] = 2\pi\chi = 0 \quad (6.3)$$

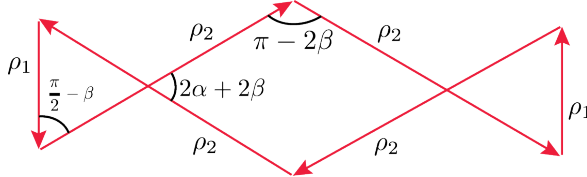


Fig. 6.6 Gauss map of the three interior vertices in the closed configuration of the unit cell. The total solid angle as a sum of each signed area is zero; thus, the interior holds no net Gaussian curvature as expected.

where the exterior angles are:

$$\alpha_{ext,1} = \pi + 2\alpha, \quad \alpha_{ext,2} = \frac{3\pi}{2} - \alpha. \quad (6.4)$$

In the open configuration, the cell is an annulus and  $\chi$  is 0. In the cell's closed configuration,  $\chi$  becomes 1. The angular defect computation becomes a calculation of spherical polygon area, denoted  $A_{quad}$  and  $A_{tri}$  for the area of a unit spherical quadrilateral and triangle, respectively:

$$A_{quad} = \sum_{i=1}^4 \alpha_i - 2\pi = 2(\pi - 2\beta) + 2(2\alpha + 2\beta) - 2\pi = 4\alpha \quad (6.5)$$

$$A_{tri} = \sum_{i=1}^3 \alpha_i - \pi = 2\left(\frac{\pi}{2} - \beta\right) + (2\alpha + 2\alpha) = 2\alpha. \quad (6.6)$$

Thus, the angular defect is

$$d(v) = 2(2\alpha) - 4\alpha = 0 \quad (6.7)$$

where the center solid angle is negative due to its clockwise direction shown in Fig. 6.4. The curvature, upon closing a cell, shifts to the exterior vertices and sums to  $2\pi$ . This is a continuous phenomenon; the spherical map changes throughout the cell's closing. By tessellating unit cells, we can take advantage of this curvature shift to construct a modular sheet with global shape through the combination of changing geometries. By imagining the spherical polygons created throughout the cell's motion, this discrete curvature approach gives us an intuitive sense of the kinematics in terms of angle defects and spherical maps to design networks of unit cells. We now turn to a vector parameterization of the cell in order to calculate the shape of a cell with a given geometry.

### 6.2.1 Vector Parameterization

As the topology is fixed, we analyze the geometry of the cell using the vector parameterization shown in Fig. 6.1. Using vector analysis, we can produce geometric relationships between the cell's components for use in structural design. By placing vectors along hinge lines and the hole edges, we can keep track of the facet positions throughout the cell's motion. The Rodrigues rotation formula is a straightforward method of rotating a general vector  $\mathbf{v}$  about an axis  $\mathbf{k}$  by angle  $\theta$  according to the right-hand rule [79]

$$\mathbf{v}_{\text{rot}} = \mathbf{v} \cos \theta + (\mathbf{k} \times \mathbf{v}) \sin \theta + \mathbf{k}(\mathbf{k} \cdot \mathbf{v})(1 - \cos \theta). \quad (6.8)$$

When the unit cell is in the closed configuration, we find a relationship between the

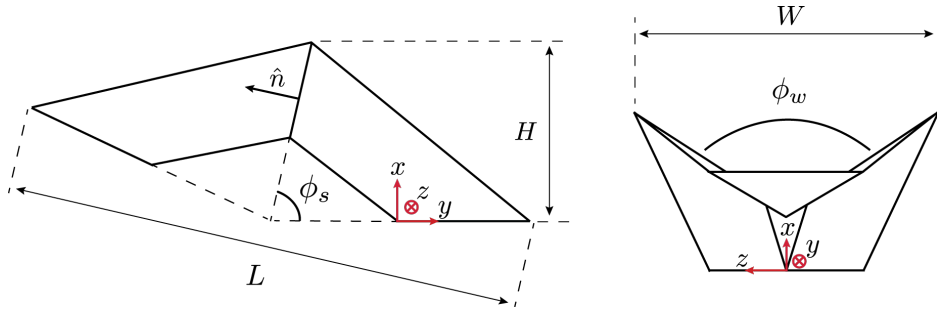


Fig. 6.7 Side and front view of the unit cell with parametric values shown.

dihedral angles,  $\rho_i$  and sector angles,  $2\beta$  and  $\frac{\pi}{2} - \beta$ , for one half of a cell where  $\rho_2$  is a function of  $\alpha$  and  $\beta$

$$\cos(\rho_{2,\text{closed}}) = \frac{\sin(\alpha + 2\beta) - \sin \alpha}{2 \sin \alpha \cos^2 \beta + 2 \cos \alpha \cos \beta \sin \beta}. \quad (6.9)$$

For the closed cell, we find the angle,  $\phi_w$  between the normalized vectors  $\hat{k}_2$  and  $\hat{k}_4$  that span the middle plane

$$\begin{aligned} \hat{k}_2 \cdot \hat{k}_4 &= \cos \phi_w \\ &= 4 \cos^2 \beta - 2 \cos^4 \beta - 4 \cos^2 \beta \cos \rho_{2,\text{closed}} \\ &\quad + 4 \cos^4 \beta \cos \rho_{2,\text{closed}} - 2 \cos^4 \beta \cos^2 \rho_{2,\text{closed}} - 1 \end{aligned} \quad (6.10)$$

where  $\rho_{2,\text{closed}}$  is the dihedral angle in the closed configuration. Substituting Eqn (6.9) into Eqn (6.10), we find  $\phi_w$  as a function on  $\alpha$  and  $\beta$  only

$$\cos \phi_w = -\frac{\cos 2\beta - \cos 2\alpha + \sin 2\alpha \sin 2\beta}{\cos(2\alpha + 2\beta) - 1}. \quad (6.11)$$

For each half of the unit cell to match, the angle,  $\phi_w$  spanned in the middle plane must match. For the singly-symmetric cell, this condition is violated. From Eqn (6.11), we see that changing  $\alpha$  while holding  $\beta$  constant will lead to a twisting of the cell's facets on the order of the change in  $\alpha$  due to the change in  $\phi_w$ . Changing the length of one side of the unit cell changes  $\cos \alpha$ , stretching one side of the cell and removing the second plane of symmetry, leading to twisting of the facets. By keeping the antisymmetric change small, we can limit the facet twisting to a trivial level. While the symmetry formula yields zero mobility for the singly-symmetric unit cell, through experimentation we find very small compliance in the cell when it is moved into the closed position shown in Fig. 6.13. With apt material selection and geometric design, it may prove useful for morphing structures despite its necessary deformation. By attaching a local coordinate system shown in Fig. 6.1, we find relationships for  $H$  and  $W$  shown in Fig. 6.7 throughout the cell's motion where

$$H = |\sin \rho_2(l \sin(\alpha + \beta) + b \cos \beta)|$$

$$\begin{aligned} W = & 2l|\sin \alpha - \cos^2 \beta \sin \alpha + \cos^2 \beta \sin \alpha \cos \rho_2| \\ & - \cos \alpha \cos \beta \sin \beta + \cos \alpha \cos \beta \sin \beta \cos \rho_2| \\ & + 2b|\cos^2 \beta \cos \rho_2 - \cos^2 \beta + 1| \end{aligned} \quad (6.12)$$

for the height and width, respectively, of the cell throughout its deployment. The middle plane spanned by the hinges  $k_1$  and  $k_4$  is described by the normal  $\hat{n}$ , shown in Fig. 6.7. We find  $\hat{n}$  using the cross product of  $k_1$  and  $k_2$  such that

$$\hat{n} = \begin{bmatrix} \frac{\sin \beta \sqrt{1-\cos \rho_2}}{\sqrt{(\cos^2 \beta \cos \rho_2 - \cos^2 \beta + 2)}} \\ -\frac{\sin \rho_2}{\sqrt{(1-\cos \rho_2)(\cos^2 \beta \cos \rho_2 - \cos^2 \beta + 2)}} \\ 0 \end{bmatrix}. \quad (6.13)$$

We find a relationship for the middle plane angle,  $\phi_s$ , shown in Fig. 6.7 as a function of  $\hat{n}$

$$\phi_s = \frac{\pi}{2} - \arccos(\hat{n} \cdot -\hat{y}). \quad (6.14)$$

where  $\hat{y}$  is the unit vector in the  $y$  coordinate direction. Computing this relationship for  $\phi_s$  yields

$$\cos(\phi_s) = \frac{\sqrt{\frac{4 \cos(2\alpha+2\beta)-4 \cos 2\beta}{\cos 2\alpha-2 \cos 2\beta+2 \cos(2\alpha+2\beta)+\cos(2\alpha+4\beta)-2}}}{\sqrt{\frac{3 \sin(\alpha+\beta)-\sin(\alpha-\beta)}{\sin(\alpha+\beta)}} \sqrt{\frac{\sin \alpha}{\sin \alpha+\sin(\alpha+2\beta)}}}. \quad (6.15)$$

Using this relationship, we can find an expression for the length of the cell

$$L = 2R_z^{\phi_s}((|d_1| + |k_1| + |k_2|) * \hat{y}) \quad (6.16)$$

where  $R_z^{\phi_s}$  is a rotation around the  $z$  axis by  $\phi_s$  and  $*$  is element-wise multiplication. We leave this expression in its symbolic form as the equations become quite long. The process to calculate these geometric relationships numerically is straightforward.

### 6.3 Linkage Analysis

To analyze the kinematics, we use a modified form of the Denavit-Hartenberg parameters [9]. For the kirigami cell where the structure begins in a flat configuration where all adjacent fold axes meet at a point, the protocol outlined in Section 4.2 requires only rotations around two axes, as shown in Fig. 4.2, where the sector angles  $\alpha$  and fold angles  $\theta$  about the  $x$  and  $z$  axes shown in Fig. 4.2 adhere to the following relationships

Table 6.4 Denavit-Hartenberg parameters for the general 6R kirigami linkage.

Link	$\alpha$	$a$	$\theta$	$d$
1	$\frac{\pi}{2} - \beta$	0	$\rho_2$	$d$
2	$\frac{\pi}{2} - \beta$	0	$\rho_1$	0
3	$2\beta$	0	$\rho_2$	$d$
4	$\frac{\pi}{2} - \beta$	0	$\rho_2$	$d$
5	$\frac{\pi}{2} - \beta$	0	$\rho_1$	0
6	$2\beta$	0	$\rho_2$	$d$

To simplify the analysis we set  $d$  to 0 for all links, effectively shrinking the rhombus hole to a point, converting the kirigami cell into a degree-6 origami vertex. This way we simplify our calculations to focus on the angle relationships, summarized as

$$\begin{aligned} \alpha_1 = \alpha_2 = \alpha_4 = \alpha_5 &= \frac{\pi}{2} - \beta, \alpha_3 = \alpha_6 = 2\beta \\ a_i &= 0 \\ \theta_1 = \theta_3 = \theta_4 = \theta_6 &= \rho_2, \theta_2 = \theta_5 = \rho_1 \\ d_i &= 0 \end{aligned} \tag{6.17}$$

Compared to the Bricard linkages listed in Table 4.2, the kirigami linkage is a type of plane-symmetric linkage as confirmed from the mobility approach in Section 6.1. Using these parameters, we compute transformation matrices between each of the six coordinate systems. Our loop closure condition based on the  $C_s$  symmetry of the cell,

$$R_{12}R_{23}R_{34} = R_{16}R_{65}R_{54} \tag{6.18}$$

yields six equations where  $R_{ij}$  is the rotational transformation matrix from coordinate system  $i$  to  $j$ , a simplified form of the matrix  $T$ . As there is one independent geometric parameter for the sector angles,  $\beta$ , and two parameters,  $\rho_1$  and  $\rho_2$ , for the hinge angles, there is only one independent loop closure equation:

$$\begin{aligned} &\sin \rho_1 \sin \rho_2 + \sin^3 \beta + \cos 2\beta \sin \beta \cos \rho_2 \\ &+ \sin^3 \beta \cos \rho_1 \cos^2 \rho_2 + \cos 2\beta \sin \beta \cos \rho_1 \cos \rho_2 \\ &= \\ &\cos^2 \beta \sin \beta \cos \rho_1 - \sin \beta \cos \rho_1 \sin^2 \rho_2 \\ &- 2 \cos^2 \beta \sin \rho_1 \sin \rho_2 - \cos^2 \beta \sin \beta \cos^2 \rho_2 - 2 \sin^2 \beta \cos \rho_2 \sin \rho_1 \sin \rho_2. \end{aligned} \tag{6.19}$$

This relationship between the three independent angular parameters of the kirigami unit cell serves as an input-output relationship. By defining the geometry of the cell through  $\beta$ , we can solve for the unknown hinge angle given a certain configuration. This relationship can be plotted as an isosurface of possible configurations for the linkage as shown in Fig. 6.8. The function is  $2\pi$  periodic as we would expect, though for physical solutions we assume that  $\rho_1$  is between  $-\frac{\pi}{2}$  and 0,  $\rho_2$  is between 0 and  $\frac{\pi}{2}$ , and  $\beta$  is between 0 and  $\frac{\pi}{2}$ . The isosurface visualizes the solution space of these parameters. As we can see, there are solutions for all  $\beta$  beginning from  $(\rho_1, \rho_2) = (0, 0)$  as well as a separate solution set beginning from  $\beta = \frac{\pi}{4}$ . By choosing two variables,

we can numerically solve for the third, which allows us to completely characterize our unit cell in any geometry and configuration. For a given  $\beta$ , there exists a contour of solutions as a function of the kinematic variables, the kinematic path. It is important to visualize these contours to find singularities in the paths. For this linkage, there are no discontinuities for predefined  $\beta$ .

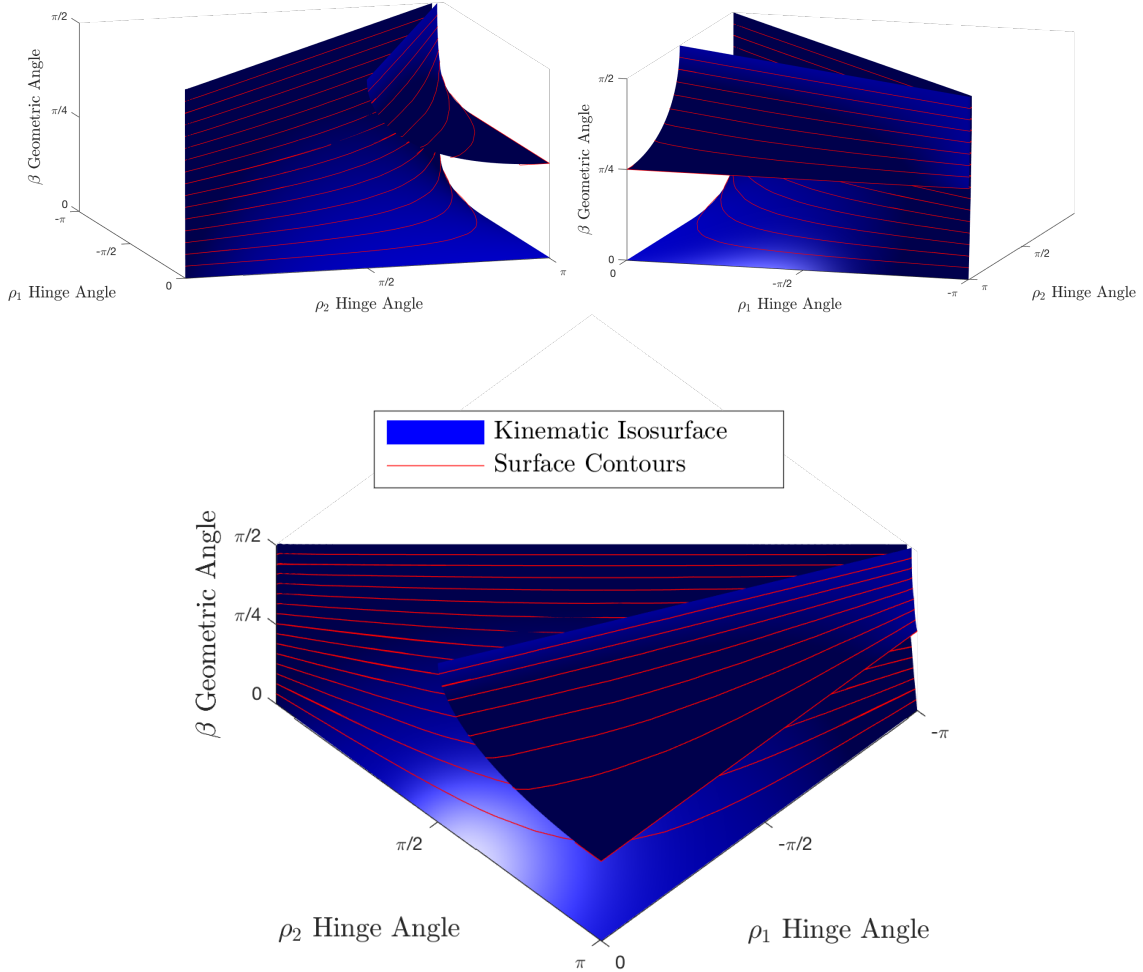


Fig. 6.8 Three views of the three-dimensional isosurface shown in blue, which provides all continuous solutions given a geometric quantity  $\beta$  for the linkage as a function of  $\rho_1$  and  $\rho_2$ . Contours on the surface are shown in red.

## 6.4 Octopus Networks

Given a single degree of freedom unit cell, we explore tessellations of this cell, or linkage networks. Beginning in one dimension, we can tile the cells end-to-end to

achieve an  $n$  degree of freedom structure with  $n$  connected cells. This structure can take  $2^n$  configurations seeing as shown in Fig. 6.9. By snubbing the corners of the octopus cell, we can tile the octagons by rotating the fold lines of the original cell. This tessellation is one degree of freedom regardless of the number of cells in the network. The hinge lines provide constraints along each edge which sets the configuration of the neighboring cell. We note that given the additional, non-actuated “holes” in this octagonal tessellation, double curvature may be achieved using non-regular cells, as shown in Fig. 6.10. However, this is not “pure” kirigami as we have previously defined given the additional voids in the sheet. Utilizing the angle defined by the geometric parameters of the cell, we develop a ring structure of one degree of freedom which lifts out of plane upon closing the voids in the cells. The radius and height of this structure can be controlled simply by the geometry of the individual cells and the number included in the tessellation as shown in Fig. 6.11. To test the feasibility of

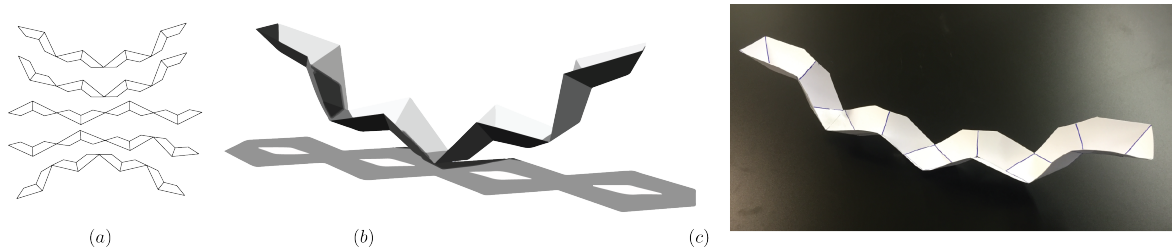


Fig. 6.9 (a) For a one dimensional tessellation with  $n$  units, we have  $2^n$  configurations, with five shown. By adjusting the geometry of the unit, we can create tessellations in a range of shapes. (b) Rendering of one configuration. (c) Physical prototype.

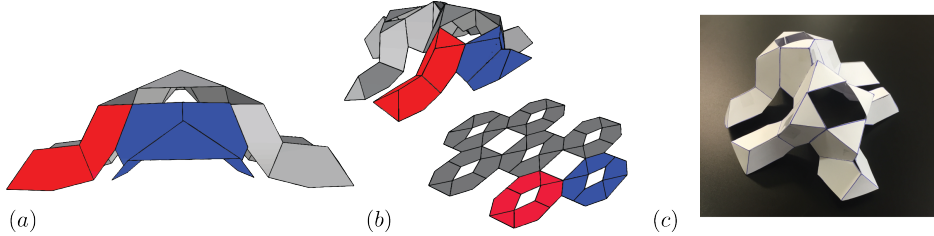


Fig. 6.10 A possible tessellation in two dimensions. All units are closed in the same sense here, approximating a doubly curved sheet. The tessellation uses two unique unit cells shown in red and blue, with hinge lines rotated by  $\frac{\pi}{2}$ . (a) Side view of the tessellation. (b) Isometric view with the unfolded configuration. (c) Physical model.

physical cells, we fabricate a unit cell from 3mm high-density polyethylene (HDPE)

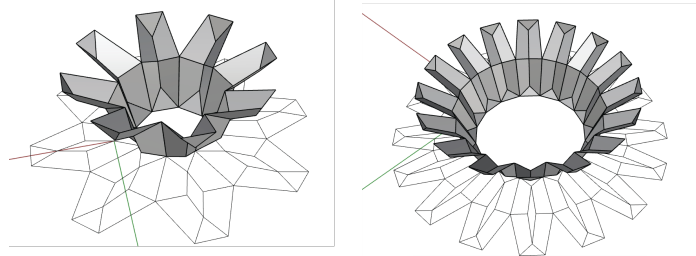


Fig. 6.11 (a) Design for an 8 cell octopus ring. (b) Design for a 16 cell octopus ring. (c) 8 cell physical prototype. (d) 16 cell physical prototype.

using a Roland MDX-40 micro-milling machine. The cell functions as expected with hinges of 1mm thickness. The physical cell is shown in the flat and deployed states in Fig. 6.12. For tessellations, a larger CNC machine could be used to produce a meter-scale tessellation in a short time. We wish to tessellate the 6R kirigami cell

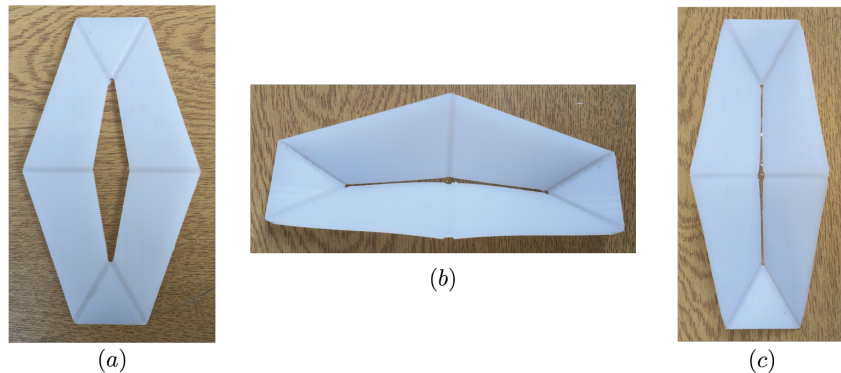


Fig. 6.12 (a) Top view of the cell in the open configuration. (b) Side view of the cell in the closed configuration. (c) Top view of the cell in the closed configuration.

without the addition of extra holes as in the case of the 2D octagonal tessellation. To achieve this, we design a hexagonal cell able to tile without voids in singly symmetric and doubly symmetric versions as shown in Fig. 6.14 with labeled geometric parameters. We dub this cell the “hexapus” unit. The kinematics of this cell are identical to the octopus cell; only the geometry is slightly changed, and all of the previous analysis still applies. As shown in Fig. 6.15, the hexagonal tessellation is a one degree of freedom structure capable of transforming between flat and singly-curved structures. The stiffness of the cylindrical shell shown here is based from the non-developable

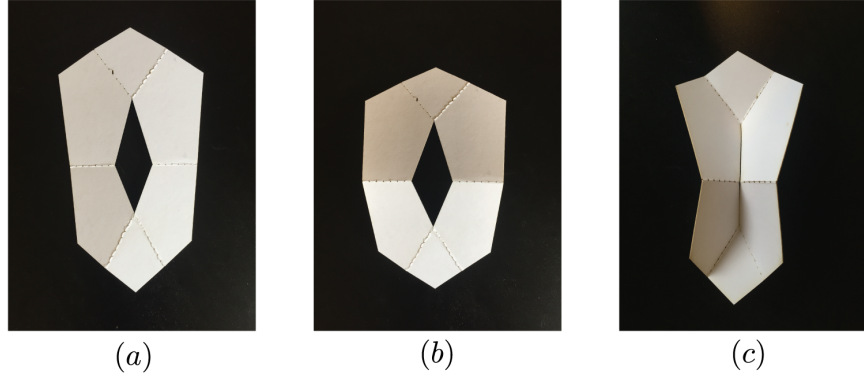


Fig. 6.13 Paper prototype of a singly-symmetric octopus cell. (a) The open configurations. (b) The mode due to geometric hinge alignment, without compliance. (c) The closed, antisymmetric mode requiring facet compliance.

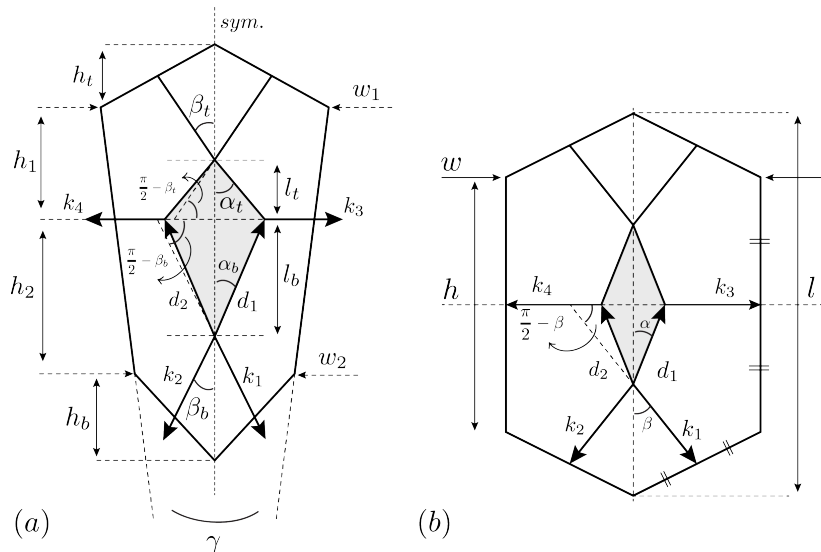


Fig. 6.14 (a) A hexagonal octopus cell with unequal side lengths and only one symmetry plane. (b) A hexagonal unit cell with two symmetry planes.

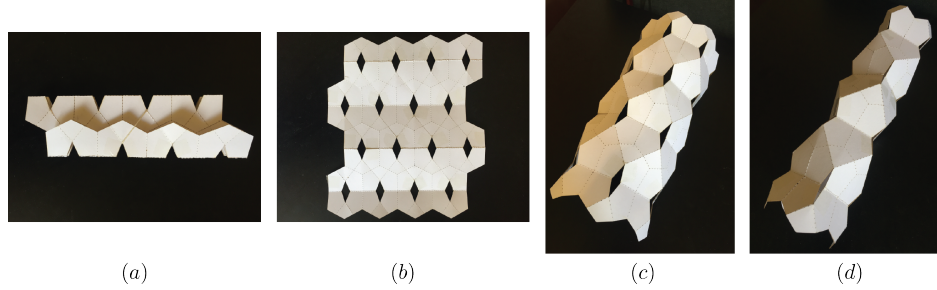


Fig. 6.15 Design for a 2D tessellation of equal-sided hexagonal cells. (a) The flat-folded state. (b) Unfurled to the planar state. (c) The partial closed folded state. (d) The final, non-developable closed cylinder state.

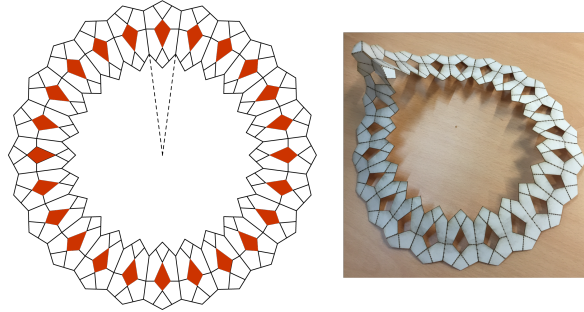


Fig. 6.16 A 1D tessellation of singly-symmetric hexagonal cells. This cell can be used to create conical forms.

vertices created during the hole gluing process. The radius and length of the cylinder can be altered by the size of the tessellation and the cells' geometric parameters. The internal shape of a tube with equal-sided hexagonal cells, where the internal cross section is a regular polygon of  $n$  sides corresponding to a tessellation  $n$  cells wide. The design parameter for a tessellation that closes exactly into a cylindrical structure is

$$\cos\left(\frac{\pi(n-2)}{n}\right) = -\frac{\cos 2\beta - \cos 2\alpha + \sin 2\alpha \sin 2\beta}{\cos(2\alpha + 2\beta) - 1} \quad (6.20)$$

invoking Eqn (6.11) and the interior angle formula for regular polygons. We can use the hexapus cell to create ring structures in the same manner as the octopus cell. This manner of tessellation can be used to create conical structures as shown in Fig. 6.16. Note that this singly symmetric unit cell will include a small degree of compliance in order to transform its shape. Thus, we can developed a tessellating kirigami unit cell that, through geometry prescription, can take a variety of forms while obeying a single

kinematic relationship. We can imagine manufacturing many of these cells for use in deployable sheets where curvature is required. Utilizing the parameterizations here, designs can be exactly calculated to achieve arbitrary, singly curved shapes. We can use both rigid folding techniques and create designs with a known amount of compliance depending on the symmetry of the desired structure.

# Chapter 7

## Conclusions and Future Work

### 7.1 Conclusions

The aim of this work is to investigate holes and understand how a sheet reacts to their opening and closing. We intended to think broadly about this question to keep our minds open to a range of conceptual tools from the most abstract to the most concrete. In this manner, we explored the consequences of holes using topology and geometry, origami and kirigami, linkages and mechanisms. We worked to develop an analytical framework for understanding kirigami tessellations with morphing possibilities. We assimilated a language for describing and characterizing kirigami towards the design of morphing sheet structures.

Using unit cell constructions and basic differential geometry, we illustrated how a shift in curvature occurs when changing homotopy groups. We outlined a framework for creating surfaces that exploit this curvature shift. These perforated structures are able to morph in a general manner using modular units. We prove that using this cellular construction, we can create singly-curved structures that are rigid-foldable, while double curvature is a product of facet compliance. By creating a network of kirigami linkages, we design several flat structures that produce an array of shapes upon local hole closings. By characterizing the motion of the unit cell, we are able to characterize the global shape of the structure. The novelty of our thinking is the transformation between states using holes. Prior work has developed the intuition for structural design using the Miura-Ori pattern, and recently kirigami has taken precedence as a route to crafting generalized shapes. Here, we draw conclusions about what shapes are possible using the kirigami technique, and push beyond known patterns and lattices to develop new unit cell geometries. By acknowledging the weakness of

a hole in a sheet, we focus on a counter-intuitive framework for shell construction to create new forms that anticipates distributed, low-power actuation.

Through the fusion of different disciplines to understand the limits and possibilities of kirigami engineering, we discovered the complexity of the form finding problem. With a new design space to explore, the avenues to explore for future research are many. The fabrication of distributed hardware systems that morph across scales is an exciting undertaking that can use the fundamental approaches described here. Generally, we hope that this work will inspire the invention of new sheet forms that incorporate the use of holes as an integral design element.

## 7.2 Future Work

The preliminary nature of this work leaves much work in the realms of analysis and experimentation. We propose avenues for further study, some of which are currently ongoing. Particularly, we discuss extended modeling techniques, mechanical analysis of the structures presented here, the form-finding problem, actuation methods for kirigami structures, and applications of transformable materials.

### 7.2.1 Modeling

This work presents several methods of analyzing kirigami sheets with respect to geometry including curvature, vector and kinematic approaches. A generalized framework combining these approaches would be useful. Some work has been done on using quaternions and dual quaternions to model origami, though to our knowledge it has not been widely adopted [80]. A more general approach to modeling large rotations in multiple dimensions is Geometric Algebra (GA), also known Clifford Algebra. Strongly motivated by geometry, GA is a vector algebra containing the concepts of quaternions and dual quaternions by providing an outer product, or wedge product, known as the geometric product. Each subspace is represented by a *multivector* of arbitrary dimension. The beauty of the system in light of origami and kirigami modeling is its coordinate-free transformations and attribution of planes to a single algebraic object called the “bivector” [81, 82]. Using GA, we can compute relationships between vectors and planes very easily, and translate our findings to an arbitrary coordinate system when necessary. There is great promise for this general language, and it may be the path towards a unified mathematical framework for describing transformable kirigami sheets.

For this project, several software tools were experimented with for the design, simulation, and fabrication of our kirigami unit cells. For the majority of the designs, the proprietary Rhinoceros software was used in conjunction with a beta version of the Grasshopper plugin, which provides parametric tools for modeling with NURBS surfaces. Additionally, several scripts written in JavaScript using the Three library were written to render designs in the browser and output in DXF format for CAD/CAM operations as shown in Fig. 7.1. While offering a great deal of flexibility and control, the JavaScript endeavor was abandoned due to time constraint, as many functions and geometric tools needed to be written. Specifically, control of polyhedral surfaces and spherical geometry is nonexistent in JavaScript, despite its computational speed, open source, and ability for fast rendering. A future project might entail designing a library for origami and kirigami design including a spherical geometry toolkit that can be executed in the browser for multi-platform use. This would prove to be a promising workflow for design, analysis and simulation, were a robust library developed.

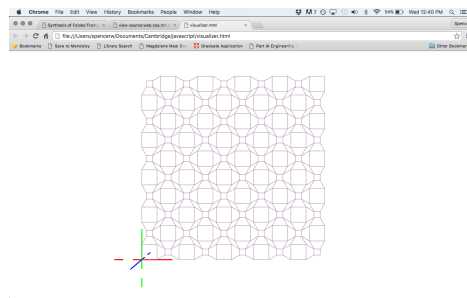


Fig. 7.1 An interactive design tool for the jellyfish geometry rendered fast in the browser using the open-source JavaScript library Three.js.

### 7.2.2 Analysis

While work has been done on the mechanical properties of the Miura-Ori pattern, the mechanical characterization of pure kirigami is known to be an important open problem [6]. Given a kirigami sheet geometry, we would like to model its stiffness and flexural modes under certain external loads in order to make a case for structural applications of these deployable structures. Our approach might be similar to that seen in the work of Schenk and Guest [1], where facets are triangulated to accommodate bending, and a matrix analysis is employed. This work would be coupled with finite element models of kirigami sheets and tubes of various geometries, and experiments using an Instron machine might confirm or deny the models used. The research objective in this case is

to show the difference in stiffness between other folded sheets and define mechanical properties such as poisson ratio and various moduli.

In the realm of manufacturing, the authors primarily used paper card and 3mm HDPE to prototype designs. The plastic prototypes were machines using a Roland RDX PCB milling machine spinning a 6mm ball-end two-flute down-spiral cutter at 5000rpm to create hinge lines and a 3mm single-flute up-spiral at 3500rpm for cutouts. To illustrate the scale-free nature of these kirigami designs, larger models should be manufactured by scaling up these manufacturing parameters and different materials should be explored, including metals and composites. A crucial step towards manufacturing kirigami sheets is to acknowledge the existence of hinge stiffness. Using a “living” hinge design relies on the elasticity and plasticity of the material to provide mobility. In this sense, a weakness of the structure gives rise to motion. We include here a brief analysis of the geometric constraint imposed by ensuring each hinge is of equal length in the structure in order for one hinge to not be energetically favored over another. This is necessary in an actuation scheme for kirigami as the actuator is imagine to have a linear motion to close the unit cell’s hole. Other hinge types of biased stiffness or locking ability should also be explored. Given the general facet of the octopus cell as shown in Fig. 7.2 with parallel sides, we derive a relationship between the geometric parameters to insure equal hinges where

$$2 - \frac{1}{\sin(\alpha)} + \frac{\sin(\beta)}{\sin(\alpha)} = \frac{\cos(\alpha)}{\cos(\beta)}. \quad (7.1)$$

Note that other manners of balancing hinge stiffness for simultaneous folding might be available. For example, perforation of the hinge joints will lower the require hinge energy. More calculations to parameterize the perforation would be necessary.

### 7.2.3 Form-Finding

The majority of this work deals with form-finding of kirigami geometries within a constrained design space. Our constraints were chiefly rigid facets, isolated hole cuttings, planarity and tiling ability of the unit cells. The difficulty of form finding is well known, though tilings of the plane using regular polygons have long been enumerated [83]. Some research has found success in finding space-filling designs using an offset method starting from tilings in two and three dimensions [84]. In this manner, the form-finding is done starting from the level of the tessellation, rather than that of the unit cell as done here. This approach may prove feasible for kirigami design as well.

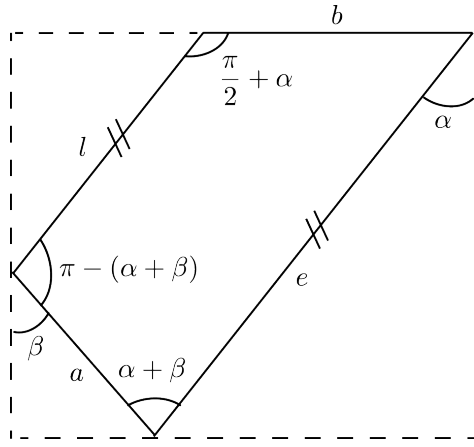


Fig. 7.2 A polygonal facet containing two hinge lines with geometric values labeled.

Is the kirigami tessellation form-finding problem tractable? If so, a numerical optimization technique could be run by combining all of the geometric constraints imposed by origami with the additional constraints and freedoms allowed by kirigami. This avenue of thinking could lead to an algorithmic form-finding technique for new kirigami tessellations. Given a target surface, we may be able find a general unfoldable tessellation with a disjoint cut tree. This is in the spirit of Tachi's work in the generalization of origami form-finding, though this would stem from the octopus or jellyfish unit cell rather than the Miura-Ori [85]. If the constraint of a repeating tessellation are relaxed, we may find quasicrystalline constructions of aperiodic kirigami using such a numerical routine. Some work has been done in the area of origami topology optimization already, though it seems only for some special cases [86].

Another area to explore is the combination of kirigami cells in two or more dimensions. By combining cells of different degrees of freedom we may be able to tune the reconfigurability of structures. By combining multiple scales of fold patterns we might create fractal tessellations. For instance, we could apply kirigami to each facet within a larger fold pattern to shift between developable and non-developable configurations. If each facet of the Miura-Ori tessellation were itself a kirigami unit, we might find a new class of transformable behavior. In three dimensions, we can think about creating kirigami volumes, or metakirigami, by stacking sheets to create solid structures.

### 7.2.4 Actuation

The goal of kirigami engineering is to provide a framework for the design of morphing shells using embedded actuators. By combining a minimum number of small, low power actuators, we can produce large geometric movement in the material to tune shape and stiffness through curvature. There are many types of actuators that could be networked for use in a kirigami sheet, but we mention a few here for further exploration.

For low power applications with a small movement, piezoelectric actuators are viable if the actuation stress is relatively low [87]. Piezoelectric actuators have been used extensively in situations where the stroke required is extremely small, on the order of microns. Piezoelectric kirigami might be suited to micro-scale applications where high accuracy is required. For higher actuation stress, shape-memory alloys (SMA) are popular. Most commonly, nickel-titanium wire is used by applying a temperature or voltage gradient across the wire, changing its chemical composition to induce strains up to 8% [88]. Nickel-Titanium wire actuators have long been used in robotics to achieve high power-to-weight ratio movement [89]. Within origami, SMAs are a popular choice for activating folding designs for peristaltic motion [90–92]. To amplify the stroke of the wire after applying a current to cause a temperature change, the wires are often coiled to form a spring-like linear actuator.

A magnetic-based actuator that shows the most promise in self-assembling structures is the electropermanent magnetic device. Combining permanent magnetic materials with high magnetic coercivity and a ferromagnetic material with low coercivity acting as an electromagnet, a magnetic switch can be designed by altering the direction of current through the electromagnet. In one direction, the magnetic poles of the two materials are aligned, generating an internal field. Pushing current in the opposite through the electromagnet will switch its poles, forcing the magnetic field to flow external to the permanent magnet, allowing it to attract nearby magnetic objects. In this manner, a switch is produced that requires a meager amount of current scaling with the volume of the magnetic devices involved [93]. These actuators have been used with great success in self-assembling cube robots [94]. We imagine employing them as geometric “switches” to change the kirigami’s configuration between on and off, or open and closed, states.

The difficulty with these small actuators is the length of the stroke and the feasible power output. The stiffness of hinges and the motions involved with changing the kirigami shape are non-negligible for physical materials. One method to circumvent the energy require to deform the kirigami from its flat state is to create a zero-stiffness kirigami. Zero stiffness devices or statically balanced mechanisms are well known, such

as the Anglepoise lamp or the Steadicam. Through static balancing, we can design a neutrally stable structure which is able to change shape without applied load. Of course, this is a theoretical situation due to pre-stress of the material, but it has been successfully realized [95, 96]. By applying the concept of zero-stiffness through the use of spring elements or pre-strain to the kirigami to create a form of kirigami tensegrity where small local changes with minimal load effect the global shape, we can realize low-power mechanisms for large geometric deformations. This avenue for further work requires a stiffness description of the structure as a whole and the exploitation of its constant potential energy. [97, 98].

### 7.2.5 Applications

Using our kirigami design scheme in conjunction with the aforementioned actuators, there are a range of applications for such dynamic devices. The movement between flat, or straight, and curved states is reminiscent of an undulatory motion. This locomotion scheme is commonly seen in aquatic life such as the jellyfish, the octopus, or the manta ray. Research to quantify manta ray locomotion has been done, and attempts at modeling this motion have been made using collapsing rhombus elements[99, 100]. Issues arise due to the complexity and bulk of these devices to achieve such a fluid motion. We believe that kirigami sheets with embedded actuation are a step closer to achieving organic locomotion.

Robotic locomotion depends on a feedback control system focused on the robot's own configuration. Another application for morphing kirigami is using feedback from the environment to change the shape of objects. By gathering inputs from the environment from a sensor network and feeding that data into the actuation network of the kirigami, we can imagine creating a structure with powerful responsiveness. This reactive structure might be used in an architectural or solar energy realm to change the exposed surface area of a structure. It could also be used to dynamically tune the stiffness of a corrugation. The key to these concepts is the geometric design of a structure that includes space for actuation, such as the rhombus holes in the designs presented here. These holes require simply a linear movement to change the global shape of the structure, opening a range of applications for experimentation.



# References

- [1] Mark Schenk and Simon D. Guest. Folded textured sheets. In *Proc. Int. Assoc. Shell Spat. Struct. Symp.*, number October, pages 2328–2336, 2010.
- [2] Aaron Lamoureux, Kyusang Lee, Matthew Shlian, Stephen R Forrest, and Max Shtein. Dynamic kirigami structures for integrated solar tracking. *Nat. Commun.*, 6:8092, 2015.
- [3] J. Eddie Baker. An analysis of the Bricard linkages. *Mech. Mach. Theory*, 15(4):267–286, 1980.
- [4] Jayavardhana Gubbi, Rajkumar Buyya, and Slaven Marusic. Internet of Things ( IoT ): A Vision , Architectural Elements , and Future Directions. *Futur. Gener. Comput. Syst.*, 29(1):1–19, 2013.
- [5] S. E. Ahnert, I. G. Johnston, T. M A Fink, J. P K Doye, and A. A. Louis. Self-assembly, modularity, and physical complexity. *Phys. Rev. E - Stat. Nonlinear, Soft Matter Phys.*, 82(2):1–9, 2010.
- [6] Toen Castle, Yigil Cho, Xingting Gong, Euiyeon Jung, Daniel M. Sussman, Shu Yang, and Randall D. Kamien. Making the cut: lattice kirigami rules. *Phys. Rev. Lett.*, 113(24):1–5, 2014.
- [7] Koryo Miura. A Note on Intrinsic Geometry of Origami, 1989.
- [8] Scott Waitukaitis and Martin Van Hecke. Origami building blocks: Generic and special four-vertices. *Phys. Rev. E - Stat. Nonlinear, Soft Matter Phys.*, 93(2):1–8, 2016.
- [9] Sarah-Marie Belcastro and Thomas C. Hull. Modelling the folding of paper into three dimensions using affine transformations. *Linear Algebra Appl.*, 348(1-3):273–282, 2002.
- [10] Tomohiro Tachi. Simulation of rigid origami. *Origami*, 4:175–187, 2006.
- [11] Tomohiro Tachi. Freeform variations of origami. *J. Geom. Graph.*, 14(2):203–215, 2010.
- [12] Mark Schenk and Simon D. Guest. Geometry of Miura-folded metamaterials. *Proc. Natl. Acad. Sci.*, 110(9):3276–3281, 2013.
- [13] Z. Y. Wei, Z. V. Guo, L. Dudte, H. Y. Liang, and L. Mahadevan. Geometric Mechanics of Periodic Pleated Origami. *Phys. Rev. Lett.*, 110(21):215501, 2013.

- [14] J M Gattas, W Wu, and Z You. Miura-base rigid origami: parameterizations of first-level derivative and piecewise geometries. *J. Mech. Des.*, 135(11):111011, 2013.
- [15] X Zhou, H Wang, and Z You. Design of three-dimensional origami structures based on a vertex approach. *Proc. R. Soc. A Math. Phys. Eng. Sci.*, 471(2181):20150407, 2015.
- [16] Levi H. Dudte, Etienne Vouga, Tomohiro Tachi, and L. Mahadevan. Programming curvature using origamitessellations. *Nat. Mater.*, (January), 2016.
- [17] Wolfgang K Schief, Alexander I Bobenko, and Tim Hoffmann. On the integrability of infinitesimal and finite deformations of polyhedral surfaces. In *Discret. Differ. Geom.*, volume 38, pages 67–93. Birkhauser Basel, 2008.
- [18] J. L. Silverberg, a. a. Evans, L. McLeod, R. C. Hayward, T. Hull, C. D. Santangelo, and I. Cohen. Using origami design principles to fold reprogrammable mechanical metamaterials. *Science (80-. ).*, 345(6197):647–650, 2014.
- [19] Arthur a. Evans, Jesse L. Silverberg, and Christian D. Santangelo. Lattice mechanics of origami tessellations. *Phys. Rev. E*, 92(1):013205, 2015.
- [20] Bryan Gin-ge Chen, Bin Liu, Arthur A. Evans, Jayson Paulose, Itai Cohen, Vincenzo Vitelli, and C. D. Santangelo. Topological mechanics of origami and kirigami. *arXiv Prepr. arXiv1508.00795*, 2:1–11, 2015.
- [21] J. F. Sadoc, N. Rivier, and J. Charvolin. Phyllotaxis: A non-conventional crystalline solution to packing efficiency in situations with radial symmetry. *Acta Crystallogr. Sect. A Found. Crystallogr.*, 68(4):470–483, 2012.
- [22] Z You and S Pellegrino. Foldable bar structures. *Int. J. Solids Struct.*, 34(15):1825–1847, 1997.
- [23] K. Zhang and J. S. Dai. Reconfiguration of the plane-symmetric double-spherical 6R linkage with bifurcation and trifurcation. *Proc. Inst. Mech. Eng. Part C J. Mech. Eng. Sci.*, 230(3):473–482, 2016.
- [24] Y. Chen and Z. You. An Extended Myard Linkage and its Derived 6R Linkage. *J. Mech. Des.*, 130(5):052301, 2008.
- [25] Y. Chen and Z. You. Mobile assemblies based on the Bennett linkage. *Proc. R. Soc. A Math. Phys. Eng. Sci.*, 461(2056):1229–1245, 2005.
- [26] Yan Chen, Zhong You, and Tibor Tarnai. Threefold-symmetric Bricard linkages for deployable structures. *Int. J. Solids Struct.*, 42(8):2287–2301, 2005.
- [27] Ketao Zhang and Jian S. Dai. Classification of Origami-Enabled Foldable Linkages and Emerging Applications. In *Vol. 6B 37th Mech. Robot. Conf.*, volume 6 B, page V06BT07A024, 2013.
- [28] Maryam Eidini. Zigzag-base folded sheet cellular mechanical metamaterials. *arXiv Prepr.*, 6:15, 2015.

- [29] M Eidini and G H Paulino. Unraveling metamaterial properties in zigzag-base folded sheets. *Sci. Adv.*, 1(8):e1500224–e1500224, 2015.
- [30] Kazuya Saito, Akira Tsukahara, and Yoji Okabe. Designing of self-deploying origami models using geometrically misaligned crease patterns. In *Proc. ASME 2014 Int. Des. Eng. Tech. Comput. Inf. Eng. Conf. IDETC/CIE 2014 August 17-20, 2014*, pages 1–9, 2016.
- [31] J. M. Gattas and Z. You. Design and digital fabrication of folded sandwich structures. *Autom. Constr.*, 63:79–87, 2016.
- [32] Hiromi Yasuda, Thu Yein, Tomohiro Tachi, Koryo Miura, and Minoru Taya. Folding behaviour of Tachi – Miura polyhedron bellows. *Proc. R. Soc. A Math. Phys. Eng. Sci.*, 469:201303(August):1–18, 2013.
- [33] Evgueni T Filipov, Tomohiro Tachi, and Glauco H Paulino. Origami tubes assembled into stiff, yet reconfigurable structures and metamaterials. *Proc. Natl. Acad. Sci. U. S. A.*, 112(40):12321–12326, 2015.
- [34] E. T. Filipov, G. H. Paulino, and T. Tachi. Origami tubes with reconfigurable polygonal cross-sections. *Proc. R. Soc. A Math. Phys. Eng. Sci.*, 472(2185):20150607, 2016.
- [35] Kenneth C Cheung, Tomohiro Tachi, Sam Calisch, and Koryo Miura. Origami interleaved tube cellular materials. *Smart Mater. Struct.*, 23(9):094012, 2014.
- [36] D.a. Huffman. Curvature and Creases: A Primer on Paper. *IEEE Trans. Comput.*, C-25(10):1010–1019, 1976.
- [37] Martin Kilian, Simon Flöry, Zhonggui Chen, Niloy J. Mitra, Alla Sheffer, and Helmut Pottmann. Curved folding. *ACM Trans. Graph.*, 27(3):1, 2008.
- [38] Marcelo a Dias and Christian D Santangelo. The shape and mechanics of curved-fold origami structures. *EPL (Europhysics Lett.)*, 100(5):54005, 2012.
- [39] Joseph M. Gattas and Zhong You. Miura-Base Rigid Origami: Parametrizations of Curved-Crease Geometries. *J. Mech. Des.*, 136(12):121404, 2014.
- [40] Y. Chen, R. Peng, and Z. You. Origami of thick panels. *Science (80-. ).*, 349(6246):396–400, 2015.
- [41] R.G. Hutchinson, N. Wicks, A.G. Evans, N.A. Fleck, and J.W. Hutchinson. Kagome plate structures for actuation. *Int. J. Solids Struct.*, 40(25):6969–6980, 2003.
- [42] Mila Boncheva, Stefan a Andreev, L Mahadevan, Adam Winkleman, David R Reichman, Mara G Prentiss, Sue Whitesides, and George M Whitesides. Magnetic self-assembly of three-dimensional surfaces from planar sheets. *Proc. Natl. Acad. Sci. U. S. A.*, 102(11):3924–3929, 2005.
- [43] E Hawkes, B An, N M Benbernou, H Tanaka, S Kim, E D Demaine, D Rus, and R J Wood. Programmable matter by folding. *Proc. Natl. Acad. Sci. U. S. A.*, 107(28):12441–5, 2010.

- [44] Qi Ge, Conner K Dunn, H Jerry Qi, and Martin L Dunn. Active origami by 4D printing. *Smart Mater. Struct.*, 23(9):1–15, 2014.
- [45] Edwin A Peraza-Hernandez, Darren J Hartl, Richard J Malak Jr, and Dimitris C Lagoudas. Origami-inspired active structures: a synthesis and review. *Smart Mater. Struct.*, 23(9):094001, 2014.
- [46] M Pagitz and J Bold. Shape-changing shell-like structures. *Bioinspir. Biomim.*, 8(1):016010, 2013.
- [47] Ramses V. Martinez, Carina R. Fish, Xin Chen, and George M. Whitesides. Elastomeric Origami: Programmable Paper-Elastomer Composites as Pneumatic Actuators. *Adv. Funct. Mater.*, 22(7):1376–1384, 2012.
- [48] Johannes T.B. Overvelde, Twan A de Jong, Yanina Shevchenko, Sergio A Becerra, George M Whitesides, James C Weaver, Chuck Hoberman, and Katia Bertoldi. A three-dimensional actuated origami-inspired transformable metamaterial with multiple degrees of freedom. *Nat. Commun.*, 7:10929, 2016.
- [49] Stephen Daynes, Richard S Trask, and Paul M Weaver. Bio-inspired structural bistability employing elastomeric origami for morphing applications. *Smart Mater. Struct.*, 23(12):125011, 2014.
- [50] Jun Ueda, Thomas Secord, and H Harry Asada. Piezoelectric Cellular Actuators Using Nested Rhombus Multilayer Mechanisms. In *Dyn. Syst. Control Conf.*, pages 203–210, 2008.
- [51] M. Santer and S. Pellegrino. Compliant multistable structural elements. *Int. J. Solids Struct.*, 45(24):6190–6204, 2008.
- [52] Matthew Santer and Sergio Pellegrino. Concept and design of a multistable plate structure. *J. Mech. Des.*, 133(8):081001, 2011.
- [53] A. I. Egunov, J. G. Korvink, and V. A. Luchnikov. Polydimethylsiloxane bilayer films with an embedded spontaneous curvature. *Soft Matter*, 12(1), 2016.
- [54] Marcelo A. Dias, James A. Hanna, and Christian D. Santangelo. Programmed buckling by controlled lateral swelling in a thin elastic sheet. *Phys. Rev. E*, 84(3):1–7, 2011.
- [55] Jemal Guven, J. A. Hanna, Osman Kahraman, and Martin Michael Müller. Dipoles in thin sheets. *Eur. Phys. J. E*, 36(9):18, 2013.
- [56] G. A. Vliegenthart and G. Gompper. Forced crumpling of self-avoiding elastic sheets. *Nat. Mater.*, 5(3):216–221, 2006.
- [57] Enrique Cerda and L. Mahadevan. Conical Surfaces and Crescent Singularities in Crumpled Sheets. *Phys. Rev. Lett.*, 80(11):2358–2361, 1998.
- [58] S.M. Farmer and C.R. Calladine. Geometry of “developable cones”. *Int. J. Mech. Sci.*, 47(4-5):509–520, 2005.

- [59] Daniel M. Sussman, Yigil Cho, Toen Castle, Xingting Gong, Euiyeon Jung, Shu Yang, and Randall D. Kamien. Algorithmic lattice kirigami: A route to pluripotent materials. *Proc. Natl. Acad. Sci. U. S. A.*, 112(24):7449–7453, 2015.
- [60] Ruikang Xie, Yan Chen, and Joseph M. Gattas. Parametrisation and application of cube and eggbox-type folded geometrics. *Int. J. Sp. Struct.*, in-press(2):99–110, 2015.
- [61] K. Saito, F. Agnese, and F. Scarpa. A Cellular Kirigami Morphing Wingbox Concept. *J. Intell. Mater. Syst. Struct.*, 22(June):935–944, 2011.
- [62] Kazuya Saito, Sergio Pellegrino, and Taketoshi Nojima. Manufacture of Arbitrary Cross-Section Composite Honeycomb Cores Based on Origami Techniques. *J. Mech. Des.*, 136(5):051011, 2014.
- [63] Cheng Lv, Hongyu Yu, and Hanqing Jiang. Archimedean spiral design for extremely stretchable interconnects. *Extrem. Mech. Lett.*, 1:29–34, 2014.
- [64] Zeming Song, Xu Wang, Cheng Lv, Yonghao An, Mengbing Liang, Teng Ma, David He, Ying-Jie Zheng, Shi-Qing Huang, Hongyu Yu, and Hanqing Jiang. Kirigami-based stretchable lithium-ion batteries. *Sci. Rep.*, 5:10988, 2015.
- [65] Yihui Zhang, Zheng Yan, Kewang Nan, Dongqing Xiao, Yuhao Liu, Haiwen Luan, Haoran Fu, Xizhu Wang, Qinglin Yang, Jiechen Wang, Wen Ren, Hongzhi Si, Fei Liu, Lihen Yang, Hejun Li, Junlong Wang, Xuelin Guo, Hongying Luo, Liang Wang, Yonggang Huang, and John a. Rogers. A mechanically driven form of Kirigami as a route to 3D mesostructures in micro/nanomembranes. *Proc. Natl. Acad. Sci.*, 112(38):201515602, 2015.
- [66] Terry C. Shyu, Pablo F. Damasceno, Paul M. Dodd, Aaron Lamoureux, Lizhi Xu, Matthew Shlian, Max Shtain, Sharon C. Glotzer, and Nicholas a. Kotov. A kirigami approach to engineering elasticity in nanocomposites through patterned defects. *Nat. Mater.*, 14(8):785–789, 2015.
- [67] Oliver Knill. A graph theoretical Gauss-Bonnet-Chern Theorem. *Elem. der Math.*, page 26, 2011.
- [68] P.A. Firby and C.F. Gardiner. *Surface Topology*. Ellis Horwood, Chichester, 2nd edition, 1991.
- [69] C. R. Calladine and J. L. Sanders. *Theory of Shell Structures*, volume 51. Cambridge University Press, 1984.
- [70] Lyuba Alboul, Gilberto Echeverria, and Marcos Rodrigues. Discrete curvatures and Gauss maps for polyhedral surfaces. *Eur. Work. Comput. Geom.*, pages 9–12, 2005.
- [71] Marshall Bern, Erik D. Demaine, David Eppstein, Eric Kuo, Andrea Mantler, and Jack Snoeyink. Ununfoldable polyhedra with convex faces. *Comput. Geom. Theory Appl.*, 24(2):51–62, 2003.
- [72] Branko Grünbaum. *Convex polytopes*. Springer, London, 2nd edition, 2003.

- [73] George H Orland. On Non-convex Polyhedral Surfaces. *Pacific J. Math.*, 15(1), 1965.
- [74] S. Pellegrino and C.R. Calladine. Matrix analysis of statically and kinematically indeterminate frameworks. *Int. J. Solids Struct.*, 22(4):409–428, 1986.
- [75] S.D. Guest and P.W. Fowler. A symmetry-extended mobility rule. *Mech. Mach. Theory*, 40(9):1002–1014, sep 2005.
- [76] P.W. Fowler and Simon D. Guest. A symmetry extension of Maxwell’s rule for rigidity of frames. *Int. J. Solids Struct.*, 37(12):1793–1804, 2000.
- [77] Gordon James. *Representations and Characters of Groups*. Cambridge University Press, Cambridge, 2nd edition, 2001.
- [78] J. Denavit and R.S. Hartenberg. A kinematic notation for lower-pair mechanisms based on matrices. *Trans. ASME. J. Appl. Mech.*, 22:215–221, 1955.
- [79] Serge Belongie. Rodrigues’ rotation formula. *MathWorld—A Wolfram Web Resource*, 1999.
- [80] W. Wu and Z. You. Modelling rigid origami with quaternions and dual quaternions. *Proc. R. Soc. A Math. Phys. Eng. Sci.*, 466(2119):2155–2174, 2010.
- [81] Christian Doran and Anthony Lasenby. Geometric Algebra for Physicists. page 578, 2003.
- [82] Richard Alan Miller. Geometric Algebra : An Introduction with Applications in Euclidean and Conformal Geometry. page 162, 2013.
- [83] Branko Grunbaum, Shephard, and Geoffrey C. Tilings by Regular Polygons. *Math. Mag.*, 50(5):227–247, 1977.
- [84] Kazuya Saito and Taketoshi Nojima. Development of Light-Weight Rigid Core Panels. *J. Solid Mech. Mater. Eng.*, 1(9):1097–1104, 2007.
- [85] Tomohiro Tachi. Generalization of rigid foldable quadrilateral mesh origami. *J. Int. Assoc. Shell Spat. Struct.*, 50(October):2287–2294, 2009.
- [86] Kazuko Fuchi and Alejandro R. Diaz. Origami Design by Topology Optimization. *J. Mech. Des.*, 135(11):111003, 2013.
- [87] J. E. Huber, N. a. Fleck, and M. F. Ashby. The selection of mechanical actuators based on performance indices. *Proc. R. Soc. A Math. Phys. Eng. Sci.*, 453(1965):2185–2205, 1997.
- [88] Jan Van Humbeeck. High temperature shape memory alloys. *Trans. ASME*, 121(January 1999):3–6, 1999.
- [89] Koji Ikuta. Shape Memory Alloy Servo Actuator System with Electrical Resistance Feedback. In *Robot. Autom.*, pages 427–430, 1988.

- [90] Sangok Seok, Cagdas Denizel Onal, Kyu Jin Cho, Robert J. Wood, Daniela Rus, and Sangbae Kim. Meshworm: A peristaltic soft robot with antagonistic nickel titanium coil actuators. *IEEE/ASME Trans. Mechatronics*, 18(5):1485–1497, 2013.
- [91] Ketao Zhang, Chen Qiu, and Jian S. Dai. Helical Kirigami-Enabled Centimeter-Scale Worm Robot With Shape-Memory-Alloy Linear Actuators. *J. Mech. Robot.*, 7(2):021014, 2015.
- [92] Wei Wang, Hugo Rodrigue, and Sung-Hoon Ahn. Deployable Soft Composite Structures. *Sci. Rep.*, 6(November 2015):20869, 2016.
- [93] A Knaian. *Electropermanent magnetic connectors and actuators : devices and their application in programmable matter*. Phd, MIT, 2010.
- [94] Kyle Gilpin and Daniela Rus. Modular robot systems from self-assembly to self-disassembly. *IEEE Robot. Autom. Mag.*, pages 38–55, 2010.
- [95] T. Tarnai. Zero stiffness elastic structures. *Int. J. Mech. Sci.*, 45(3):425–431, 2003.
- [96] Simon Guest, Elizbar Kebadze, and Sergio Pellegrino. A zero-stiffness elastic shell structure. *J. Mech. Mater. Struct.*, 6(1-4):203–212, 2011.
- [97] M. Schenk, S. D. Guest, and J. L. Herder. Zero stiffness tensegrity structures. *Int. J. Solids Struct.*, 44(20):6569–6583, 2007.
- [98] M. Schenk and Simon D. Guest. On zero stiffness. *Proc. Inst. Mech. Eng. Part C J. Mech. Eng. Sci.*, 228(10):1701–1714, 2013.
- [99] Keith W. Moored, Peter a. Dewey, Megan C. Leftwich, Hilary Bart-Smith, and Alexander J. Smits. Bioinspired Propulsion Mechanisms Based on Manta Ray Locomotion. *Mar. Technol. Soc. J.*, 45(4):110–118, 2011.
- [100] Thomas Bliss. A biomimetic approach to efficient underwater propulsion. *SPIE Newsroom*, pages 10–12, 2006.

